JOTCS B
Journal of the Turkish Chemical Society
Section: B
Chemical Engineering
TURKISH CHEMICAL SOCIETY

The Role of Stable Bicarbonate Formation on the Loss of Photocatalytic Activity of TiO_2 in Grout Media

Mert Mehmet Oymak[1], Deniz Uner*

Middle East Technical University Chemical Engineering Department, Ankara, 06531, Turkey,

Abstract: In this study, we report the photocatalytic activity of TiO_2 monitored by benzene oxidation in the grout medium. The results of the batch reaction tests indicated that the activity of TiO_2 coated on grout was substantially less than TiO_2 coated on a glass substrate. CO_2 adsorption on these samples were monitored by DRIFTS. The results reveal that the loss of activity in the grout medium was due to formation of stable carbonates-bicarbonates in highly alkaline grout media.

Keywords: Photocatalytic benzene oxidation, CO_2 Adsorption/DRIFTS, cement/grout media, dimeric form/bicarbonate, HLW/TiO_2

Submitted: August 3, 2021. **Accepted:** December 3, 2021.

Cite this: Oymak M, Uner D. The Role of Stable Bicarbonate Formation on the Loss of Photocatalytic Activity of TiO_2 in Grout Media. JOTCSB. 2022;5(1):1–8.

***Corresponding author. E-mail:** uner@metu.edu.tr.

INTRODUCTION

There is a growing market for self-cleaning and air purifying photocatalytic cementitious materials (1). Similar to cement matrix, grout matrix is also an ideal surface for photocatalytic utilization. Compared to cement matrix, grout matrices are frequently used in indoors and therefore sunlight exposure of these materials is low. However, grout applications such as patios, mosaic, stone, and tile works are aesthetic and high cost surfaces, and self-cleaning properties are desirable. Photocatalysts can be applied onto different structural supports (2), embedded in bulk (3-4). Nowadays, commercial building materials are directly coated with photocatalysts (5). The durability of the photocatalytic building materials is of both academic and commercial concern (6).

Concrete matrix, frequently encountered in buildings, is a highly alkaline environment. This high alkalinity can result in extensive amounts of CO_2 and NOx ad(ab)sorption. A recent study (7) reports that CO_2 absorption in cement matrix can compensate the CO_2 footprint of the cementitious manufacture (5). TiO_2 can also be modified with alkaline structures to increase CO_2 adsorption. Modification of TiO_2 with NH_4OH and KOH was reported to increase the total CO_2 adsorption capacity by a factor of 9 compared to the untreated sample (8). Furthermore, acidic/basic character of cementitious base materials can influence the activity of the photocatalysts. Kozlov et al. studied photocatalytic degradation of benzene and acetone with H_2SO_4 and NaOH treated samples to observe that high alkaline treatment decreased the acidic sites and photocatalytic activity of the samples (9-10). Strini et al.(11) studied photocatalytic oxidation of BTEX (Benzene, toluene, ethyl benzene and o-xylene) using P25 in Portland cement samples, comparing the activities between pure TiO_2 and TiO_2 added cementitious materials. They observed 3-10 times decrease in photocatalytic activity of P25 in cement samples when compared to pure TiO_2 activity.

Surface carbonates-bicarbonates are formed on TiO_2 surfaces under CO_2 exposure (12-21). It is known that carbon deposition changes the photocatalytic activity on TiO_2 surfaces under UV exposure or dark conditions (22). Strong Lewis acid (Ti^{4+}) and Lewis base (O^{2-}) sites favor the

1 Present address: Üsküdar University Chemical Engineering Department, İstanbul, 34662, Turkey

formation of bidentate carbonates and bicarbonate species on the surface, whereas monodentative carbonates are favored by Ti^{3+} sites (23). During photocatalytic benzene decomposition, the source of surface carbonates are the byproducts finally leading to CO and CO_2 as gaseous products (24-27).

In this article, we report activity loss due to the interactions between a commercial TiO_2 photocatalyst and its cement based environment. Our work reveals a link between carbonate-bicarbonate formation and photocatalytic activity loss on the alkaline environment of cement based samples.

EXPERIMENTAL/METHODOLOGY

A commercial TiO_2 sample (Anatase Sachtleben Hombitan LW, will be referred to as HLW from this point onwards) with a specific surface area of 11 m^2/g was used in the tests. HLW -grout sample was prepared by mixing with the grout mortar for the in-grout samples, 33 wt% water was added and the final slurry was cast in a plastic vessel (8.5 cm ID, 5 mm depth). A plain grout mortar was also prepared. The samples were cured for 28 days in a controlled atmosphere conditioned at 23 ^oC and 50% RH. On-the-grout sample was prepared by depositing 0.01 g TiO_2-deionized water solution using a syringe. On-the-glass sample was prepared by doctor blade method. The samples were air-dried for one day.

Photocatalytic benzene oxidation reaction was carried out in a homemade glass manifold (215 ml) operating in batch mode at 1 atm and room temperature. Prior to reaction measurements, the system was evacuated for 30 minutes and the reaction cell was photo-irradiated for 1 hour under vacuum. 0.2 µL of benzene was introduced to a heated manifold kept at 85 ^oC through a septum injection port and allowed to evaporate. Benzene-air mixture in gaseous form was transferred from heating system to the reaction cell through a vacuum-tight valve. The reaction products were periodically sampled through a septum by a gas-tight syringe and analyzed using a Gas Chromatograph (Varian 3900) equipped with FID and PoraplotQ capillary column. 100 W UVA (~365 nm) black light was used for photoexcitation. On the same sample, both dark and UV irradiated activities were measured. The dark experiments were done by covering the sample cell with aluminum foil while keeping the cell illuminated, to maintain identical thermal conditions.

DRIFTS (Diffuse Reflectance Infrared Fourier Transform Spectrometry) studies were performed using a Perkin Elmer (Spectrum 100 Series) Spectrometer equipped with a Pike DIFFUSIR™ DRIFTS cell connected to a home built gas manifold capable of holding vacuum up to 10^{-5} Torr connected to a Varian turbo molecular pump station. Equal amounts of samples were used in the DRIFTS cell and they were in powder form for pure TiO_2, and in the precast form for grout containing samples, which is explained in the first paragraph of experimental section. Prior to the measurements, the manifold and the cell were evacuated for 30 minutes. Subsequently, CO_2 was dosed onto sample, while monitoring the pressure by a Baratron gauge (MKS). DRIFTS spectrum was recorded after allowing system to equilibrate for 20 min. After adsorption experiments were completed, the sample was evacuated for 10 min and DRIFTS spectra were also recorded under vacuum.

RESULTS AND DISCUSSION

The photocatalytic benzene oxidation rate was measured through monitoring the concentration as a function of time (Fig. 1a). The rate estimations were based on a pseudo first order kinetics, for practical purposes without making any reference to mechanism. The time dependent disappearance of benzene from the batch reaction chamber was approximated as,

$$\ln\left(\frac{C_a}{C_{a,0}}\right) = -kt \qquad (1)$$

The reaction rate constants k can be calculated from the slope of trend lines of $\ln\left(\frac{C_a}{C_{a,0}}\right)$ vs. time graphs (Fig. 1b). The comparison of pseudo first order rate constants provides a common basis for comparing the activities of different photocatalysts and different environments (28-29).

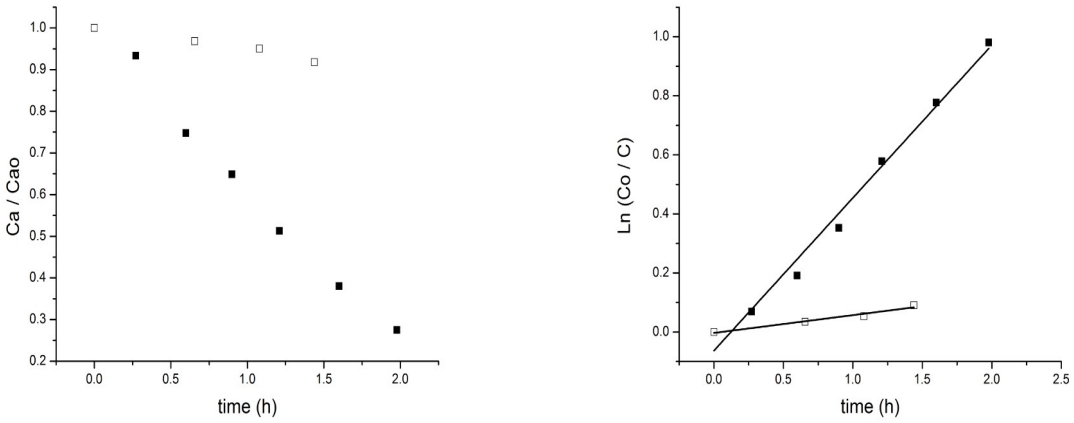

(a) **(b)**

Fig. 1: a) Benzene concentration during photocatalytic oxidation in the grout samples. The filled symbols indicate UV irradiated samples while empty symbols represent the corresponding measurements in dark. 10 wt % TiO_2 was added in the grout in both cases. b) Fig 1a is shown in the form of $\ln\left(\frac{C_{a,o}}{C_a}\right)$ vs. time.

In order to differentiate the contribution from the cement matrix, similar measurements were performed by coating the TiO_2 samples on the glass. The results were compared with the measurements of the photocatalytic activity of TiO_2 coated on the grout. The results are presented in Table 1. A comparison of the data reported in Table 1 reveals that there is substantial loss of activity on the grout.

According to the findings of an earlier publication (30) from our group, CO_2 evolution was always slower than the disappearance of C_6H_6, indicating some carbon hold-up in the structure. To test this hypothesis on the present samples, DRIFTS spectra for various HLW-grout surfaces and pure HLW and grout samples were collected (Fig. 2). IR assignments of adsorbed CO_2 on TiO_2 were made based on the literature as summarized in Table 2. The bands in DRIFTS spectra presented in Figure 2 was assigned as follows: 1800-1200 cm^{-1} region shows carbonate-bicarbonate related peaks. The absorbance in this region is low for pure grout samples. HLW integration to grout increased adsorption of CO_2 and formation of carbonates-bicarbonates substantially (Fig.2c).

Table 1: Activity comparison of HLW on glass and on grout surfaces.

	TiO_2 surface density (g/cm^2)	k_{HLW} (1/h-g cat)
On the grout	0.0005	56.6 (±16.0)
	0.0013	51.3
	0.0013	196
On the glass	0.0020	144

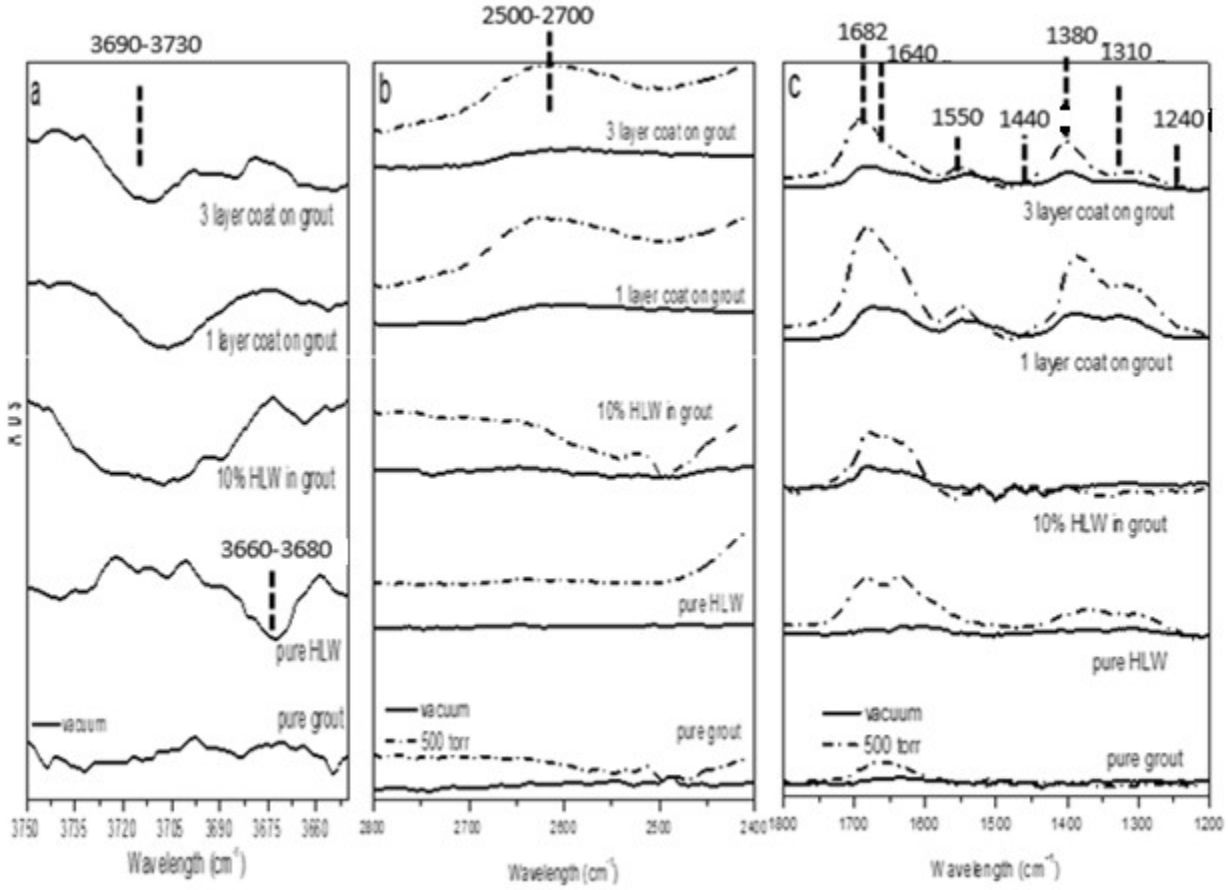

Fig. 2: DRIFTS spectra comparison of pure powder, coating and grout applications using HLW a) 3750-3650, b) 2800-2400, c) 1800-1200 cm^{-1} regions. The solid lines are collected under 500 Torr of CO_2 while dashed lines indicate the intensity after evacuation. 500 torr CO_2 data for 3750-3650 cm^{-1} region is not shown due to dominant characteristic CO_2 peaks in the region.

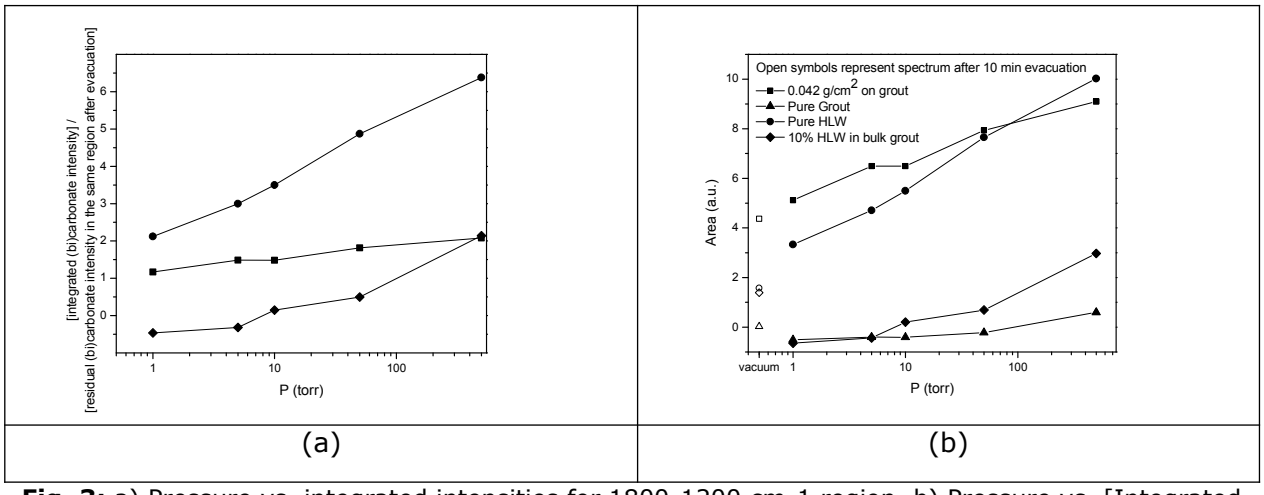

Fig. 3: a) Pressure vs. integrated intensities for 1800-1200 cm-1 region. b) Pressure vs. [Integrated (bi)carbonate intensity] / [residual (bi)carbonate intensity in the same region after evacuation]. Pure grout data in Fig 3b is not shown.

The broad peak around 2500-2700 cm^{-1} is assigned to dimeric interactions between H and OH groups of bicarbonates (Fig.2b, Table 2). This peak is observed only when HLW and grout were in intimate contact. This peak was neither observed for pure HLW nor for pure grout sample under CO_2 environment. The decrease in OH population is observed around 3700-3730 cm^{-1}

for HLW-grout and 3660-3680 cm^{-1} for pure HLW samples as negative peaks in the regions indicated. This decrease was attributed to the formation of bicarbonates over OH groups upon CO_2 adsorption. The stability of the carbonate species upon evacuation were also monitored. Surface carbonates were found to be more stable on HLW-grout than pure HLW or pure grout samples (Fig.2c). From the data in Figure 2c, it can be seen that the bands in 1200-1400 cm^{-1} range disappear upon evacuation for pure grout and 10 wt% HLW in the grout samples. These bands are however partially stable upon evacuation for pure HLW and HLW on the grout. For a semi-quantitative analysis, the area under the curve for 1800-1200 cm^{-1} region was integrated and plotted as a function of the pressure (Fig. 3a). It can be clearly seen from the isotherm data in Figure 3a that there is not an appreciable amount of (bi)carbonate hold-up on the pure grout. When TiO_2 is present, the (bi)carbonate hold-up increases (all the rest of the samples). The relative strength, i.e. stability, of the species was tested against evacuation; open symbols in Figure 3a indicate the residual intensity of the peaks after 10 min of evacuation. In Figure 3b, the isotherm data of Figure 3a (filled symbols) were plotted after they are normalized with respect to their corresponding values under vacuum (open symbols). The same data were also presented in Table 3 in terms of vacuum to 500 torr CO_2 integrated intensity ratios. The normalized values indicate that when HLW and the grout were in intimate contact, these samples hold more surface carbonate-bicarbonate species than either pure HLW or pure grout samples under vacuum conditions. However, the data presented in Fig. 3a and Fig. 2c clearly indicates that the bicarbonate formation characteristics on pure HLW and 0.042 g HLW/cm^2 coating on the grout are similar. The intensity of the bicarbonate species on pure HLW and HLW on the grout, reported in Fig. 3a, is much higher than both the corresponding intensity of pure HLW and that of HLW coated on the grout samples. The differences in the surface coverages upon evacuation were attributed to the stability of the dimeric bicarbonates.

The DRIFTS results were interpreted as there is a likelihood that a high amount of carbonate-bicarbonate species remain on TiO_2-grout matrix. The photocatalytic benzene oxidation results were interpreted as there is a significant activity loss of TiO_2 in the grout. These two observations are combined broadly to conclude that there is a surface poisoning due to stable carbonate-bicarbonate species in alkaline media.

The formation of bicarbonate species indicate the presence of basic OH groups (14). In this study, dimeric bicarbonate species were formed, which may be a sign of close proximity of OH groups on the surface of HLW-coated-grout matrix samples (Fig. 2b). These species are particularly resistant to evacuation. In addition, for the same samples, OH frequencies shift from 3660-3680 to 3730-3700 cm^{-1} region compared to pure HLW (Fig. 2a). We have to note that our measurements of reaction as well as DRIFTS were performed under conditions where water was not deliberately added to the gas streams. A recent report on an STM experiment demonstrated the importance of the film of water in CO_2 adsorption mechanism, eventually leading to formation of highly stable bicarbonates on rutile (110) (31). Furthermore, solvation effect of water decreases the energy barriers for CO_2 reduction and changes the selectivity of reaction processes on rutile (110) according to a recent first-principles calculation study (32).

A schematic representation of dimeric bicarbonate formation is given in Fig.4. Sorption takes place with initial interaction of CO_2 groups with hydroxyl groups on the surface. O-H groups make a nucleophilic attack to CO_2, forming adsorbed bicarbonate structure. This kind of bicarbonate formation is consistent with the experimental observations indicating that the OH populations decrease upon CO_2 adsorption as well.

Table 2: Peak assignments for CO_2 adsorption on TiO_2 anatase.

	Wavelength (cm^{-1})	Comments	Ref	This study
OH Stretching / Bending assignments	3735,3725,3715	ν_{OH}	10,11,12	3690-3730
	3690, 3675,3670,3665, 3640,3630(sh.)[a]	ν_{OH}	10,11, 13,12	3660-3680
	3600-3200(br.)[a]	ν_{OH} (surface and residual water)	13	3500-3000(br.)[a]
	3500-2800(br.)[a]		13	
	3350-3100(br.)[a]		10	
	1630, 1605	δ_{OH}	10,13	1640
CO_2 Assignments	3609, 3716		14	3728,3705, 3627,3600
	2375, 2360,2350, 2280[b]		12	2360,2347, 2340,2335
Carbonate / Bicarbonate Assignments	3340-3148,ν_{OH}	M–bicarbonates[c]	15	
	2620-2450,ν_{OH-O}	D-bicarbonates[c]	15	2500-2700(br.)[a]
	1702-1675,asym$\nu_{C=O}$	M–bicarbonates[c]	15	
	1672,1670	Bidentate	13,16	
	1670(sh.)[a]	Bicarbonate	14	1682
	1655-1615,asym$\nu_{C=O}$	D-bicarbonates[c]	15	
	1630	Bicarbonate	13	1640
	1632-1600	CO_3^- derivatives	10	
	1595,1578,1590-1575	Monodentate	13,16	
	1580	CO_2^- derivatives	10	1550
	1555	Bicarbonate	14	
	1410-1300	CO_3^- derivatives	10	
	1400-1370,symm$\nu_{C=O}$	D-bicarbonates[c]	15	
	1430,1420,1408	Bicarbonate	14,13	1440
	1370-1320,1359,1315	Monodentate	13,16	1380
	1346-1327,symm$\nu_{C=O}$,	M–bicarbonates[c]	15	
	1340	Bicarbonate	14	
	1320	CO_2^- derivatives	10	1310
	1300,δ_{OH-O}	D-bicarbonates[c]	15	
	(1252-1205,δ_{OH})	M–bicarbonates[c]	15	
	1243	Bidentate	13,16	
	1221,1220	Bicarbonate	14,13	1240
	1053	Bidentate	13	

[a]br.:broad peak,sh.:shoulder,[b] $^{13}CO_2$,[c]On metal oxides, M-monomeric, D-dimeric

Table 3: Carbonate bicarbonate region integrated DRIFTS intensities under vacuum, normalized with respect to their corresponding values under 500 Torr CO_2.[a] Two pure HLW experiments are averaged.

Sample	Integrated Area (Vacuum / 500 torr CO_2)
0.042 g/cm^2 coat on grout	0.48
0.014 g/cm^2 coat on grout	0.42
10% HLW in bulk grout	0.47
Pure HLW[a]	0.21
Pure grout	0.04

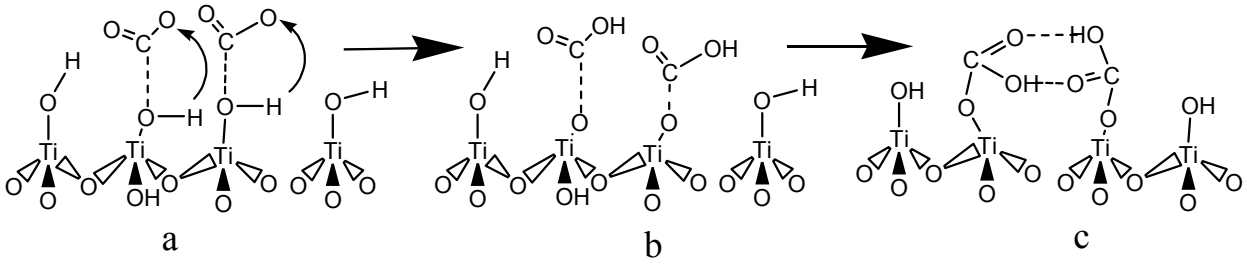

Fig. 4: Schematics of a) approach of CO_2 molecule to the surface, b) bicarbonate formation, c) dimeric bicarbonate formation.

CONCLUSIONS

The activity of the TiO_2 photocatalyst for benzene photooxidation declined by a factor of 3 when coated on a cementitious grout medium relative to the activity of a coating on a glass substrate. A detailed DRIFTS study unraveled the formation of stable carbonate-bicarbonates on TiO_2 surface in alkaline grout media. Also, dimeric bicarbonate interactions were observed on HLW-coated grout surfaces. We surmise that alkalinity in the grout can inhibit TiO_2-active sites and decrease the photocatalytic activity.

ACKNOWLEDGMENTS

Partial financial support through SANTEZ program by Kalekim A.Ş. and Turkish Ministry of Science, Industry and Technology under grant no 00336.STZ.2008-2 is acknowledged.

REFERENCES

1. M Oymak M, Uner D. Patents on photocatalyst incorporated cement based materials. Recent Patents on Catalysis (Discontinued). 2013;2(2):116–29.

2. Ramirez AM, Demeestere K, De Belie N, Mäntylä T, Levänen E. Titanium dioxide coated cementitious materials for air purifying purposes: Preparation, characterization and toluene removal potential. Building and Environment. 2010 Apr;45(4):832–8. <DOI>.

3. Aïssa AH, Puzenat E, Plassais A, Herrmann J-M, Haehnel C, Guillard C. Characterization and photocatalytic performance in air of cementitious materials containing TiO2. Case study of formaldehyde removal. Applied Catalysis B: Environmental. 2011 Aug;107(1–2):1–8. <DOI>.

4. Jimenez-Relinque E, Llorente I, Castellote M. TiO 2 cement-based materials: Understanding optical properties and electronic band structure of complex matrices. Catalysis Today. 2017 Jun;287:203–9. <DOI>.

5. Demeestere K, Dewulf J, De Witte B, Beeldens A, Van Langenhove H. Heterogeneous photocatalytic removal of toluene from air on building materials enriched with TiO2. Building and Environment. 2008 Apr;43(4):406–14. <DOI>.

6. Boonen E, Beeldens A, Dirkx I, Bams V. Durability of Cementitious Photocatalytic Building Materials. Catalysis Today. 2017 Jun;287:196–202. <DOI>.

7. Xi F, Davis SJ, Ciais P, Crawford-Brown D, Guan D, Pade C, et al. Substantial global carbon uptake by cement carbonation. Nature Geosci. 2016 Dec;9(12):880–3. <DOI>.

8. Kapica-Kozar J, Kusiak-Nejman E, Wanag A, Kowalczyk Ł, Wrobel RJ, Mozia S, et al. Alkali-treated titanium dioxide as adsorbent for CO2 capture from air. Microporous and Mesoporous Materials. 2015 Jan;202:241–9. <DOI>.

9. Kozlov D, Bavykin D, Savinov E. Effect of the Acidity of TiO2 Surface on Its Photocatalytic Activity in Acetone Gas-Phase Oxidation. Catalysis Letters. 2003;86(4):169–72. <DOI>.

10. Kozlov DV, Panchenko AA, Bavykin DV, Savinov EN, Smirniotis PG. Influence of humidity and acidity of the titanium dioxide surface on the kinetics of photocatalytic oxidation of volatile organic compounds. Russian Chemical Bulletin. 2003;52(5):1100–5. <DOI>.

11. Strini A, Cassese S, Schiavi L. Measurement of benzene, toluene, ethylbenzene and o-xylene gas phase photodegradation by titanium dioxide dispersed in cementitious materials using a mixed flow reactor. Applied Catalysis B: Environmental. 2005 Oct;61(1–2):90–7. <DOI>.

12. Yates D. Infrared studies of the surface hydroxyl groups on titanium dioxide, and of the chemisorption of carbon monoxide and carbon dioxide. The Journal of Physical Chemistry. 1961;65(5):746–53.

13. Primet M, Pichat P, Mathieu MV. Infrared study of the surface of titanium dioxides. I.

Hydroxyl groups. The Journal of Physical Chemistry. 1971;75(9):1216–20.

14. Busca G, Saussey H, Saur O, Lavalley JC, Lorenzelli V. FT-IR characterization of the surface acidity of different titanium dioxide anatase preparations. Applied Catalysis. 1985 Jan;14:245–60. <DOI>.

15. Martra G. Lewis acid and base sites at the surface of microcrystalline TiO2 anatase: relationships between surface morphology and chemical behaviour. Applied Catalysis A: General. 2000 Aug;200(1–2):275–85. <DOI>.

16. Mathieu MV, Primet M, Pichat P. Infrared study of the surface of titanium dioxides. II. Acidic and basic properties. The Journal of Physical Chemistry. 1971;75(9):1221–6.

17. Busca G, Lorenzelli V. Infrared spectroscopic identification of species arising from reactive adsorption of carbon oxides on metal oxide surfaces. Materials Chemistry. 1982 Jan;7(1):89–126. <DOI>.

18. Morterra C, Chiorino A, Boccuzzi F, Fisicaro E. A Spectroscopic Study of Anatase Properties. Zeitschrift für Physikalische Chemie. 1981 Feb 1;124(2):211–22. <DOI>.

19. Tanaka K, White J. Characterization of species adsorbed on oxidized and reduced anatase. The Journal of Physical Chemistry. 1982;86(24):4708–14.

20. Ramis G, Busca G, Lorenzelli V. Low-temperature CO2 adsorption on metal oxides: spectroscopic characterization of some weakly adsorbed species. Materials Chemistry and Physics. 1991 Sep;29(1–4):425–35. <DOI>.

21. Bhattacharyya K, Danon A, K.Vijayan B, Gray KA, Stair PC, Weitz E. Role of the Surface Lewis Acid and Base Sites in the Adsorption of CO 2 on Titania Nanotubes and Platinized Titania Nanotubes: An in Situ FT-IR Study. J Phys Chem C. 2013 Jun 20;117(24):12661–78. <DOI>.

22. Uner D, Oymak MM. On the mechanism of photocatalytic CO2 reduction with water in the gas phase. Catalysis Today. 2012 Feb;181(1):82–8. <DOI>.

23. Wu W, Bhattacharyya K, Gray K, Weitz E. Photoinduced Reactions of Surface-Bound Species on Titania Nanotubes and Platinized Titania Nanotubes: An in Situ FTIR Study. J Phys Chem C. 2013 Oct 10;117(40):20643–55. <DOI>.

24. Jacoby WA, Blake DM, Penned JA, Boulter JE, Vargo LM, George MC, et al. Heterogeneous Photocatalysis for Control of Volatile Organic Compounds in Indoor Air. Journal of the Air & Waste Management Association. 1996 Sep;46(9):891–8. <DOI>.

25. d'Hennezel O, Pichat P, Ollis DF. Benzene and toluene gas-phase photocatalytic degradation over H2O and HCL pretreated TiO2: by-products and mechanisms. Journal of Photochemistry and Photobiology A: Chemistry. 1998 Nov;118(3):197–204. <DOI>.

26. Wu W-C, Liao L-F, Lien C-F, Lin J-L. FTIR study of adsorption, thermal reactions and photochemistry of benzene on powdered TiO2. Phys Chem Chem Phys. 2001;3(19):4456–61. <DOI>.

27. Zhong J, Wang J, Tao L, Gong M, Zhimin L, Chen Y. Photocatalytic degradation of gaseous benzene over TiO2/Sr2CeO4: Kinetic model and degradation mechanisms. Journal of Hazardous Materials. 2007 Jan;139(2):323–31. <DOI>.

28. Lachheb H, Puzenat E, Houas A, Ksibi M, Elaloui E, Guillard C, et al. Photocatalytic degradation of various types of dyes (Alizarin S, Crocein Orange G, Methyl Red, Congo Red, Methylene Blue) in water by UV-irradiated titania. Applied Catalysis B: Environmental. 2002 Nov;39(1):75–90. <DOI>.

29. Stylidi M, Kondarides D, Verykios X. Pathways of solar light-induced photocatalytic degradation of azo dyes in aqueous TiO2 suspensions. Applied Catalysis B: Environmental. 2003 Feb 28;40(4):271–86. <DOI>.

30. Uner DO, Ozbek S. The deactivation behavior of the TiO2 used as a photo-catalyst for benzene oxidation. In: Studies in Surface Science and Catalysis [Internet]. Elsevier; 1999 [cited 2021 Dec 6]. p. 411–4. <URL>.

31. Song A, Skibinski ES, DeBenedetti WJI, Ortoll-Bloch AG, Hines MA. Nanoscale Solvation Leads to Spontaneous Formation of a Bicarbonate Monolayer on Rutile (110) under Ambient Conditions: Implications for CO 2 Photoreduction. J Phys Chem C. 2016 May 5;120(17):9326–33. <DOI>.

32. Yin W-J, Krack M, Wen B, Ma S-Y, Liu L-M. CO 2 Capture and Conversion on Rutile TiO 2 (110) in the Water Environment: Insight by First-Principles Calculations. J Phys Chem Lett. 2015 Jul 2;6(13):2538–45. <DOI>.

JOTCS B
Journal of the Turkish Chemical Society
Section: B
Chemical Engineering
TURKISH CHEMICAL SOCIETY

Microstructure, Texture, and Some Other Properties of Ice Creams Produced with Different Processed and Different Varieties of Pumpkins

Hatice SIÇRAMAZ and Ahmet AYAR

University of Sakarya, Department of Food Engineering, Sakarya - Turkey

Abstract: Pumpkin is a rich source of antioxidants, phenolic compounds, dietary fiber, and minerals. It is also harvested in large quantities around the world. Therefore, the present investigation was undertaken to enhance the nutritional and functional properties of ice creams by fortification of two different varieties of pumpkins – *Cucurbita moschata* and *Cucurbita maxima*. Different processes - freeze-drying, boiling, and baking - were applied to pumpkins to compare and determine the optimal processing steps. In doing so, two different concentrations were operated for each application. The health-promoting effects of pumpkins were evaluated, and their effects on the functional and sensory properties of ice creams were determined. Raw pumpkins have 24.5-31.1 % total dietary fiber (TDF), 26.2-9.0 % antioxidant content in terms of DPPH scavenging activity, and 237.5-123.9 (mg GAE / 100 g DM) total phenolic content. While TDF did not change with heat treatment, antioxidant and phenolic contents decreased slightly. Mineral substance contents were also generally not affected by the heat treatment ($P > 0.05$). As a result, all types of applications were approved for their similarity to the control sample of microstructural, textural, sensorial, and other characteristics.

Keywords: Ice cream, pumpkin, dietary fiber, phenolic compound, antioxidant.

Submitted: December 26, 2021. **Accepted:** April 11, 2022.

Cite this: Sıçramaz H, Ayar A. Microstructure, Texture, and Some Other Properties of Ice Creams Produced with Different Processed and Different Varieties of Pumpkins. JOTCSB. 2022;5(1):9–20.

***Corresponding author. E-mail:** haticesicramaz@sakarya.edu.tr.

INTRODUCTION

Ice cream is a universally accepted valuable product that is rich in calcium and protein. While it's a sweet product, flavoring ingredients like fruits are usually demanded in ice creams. The addition of fruits brings additional nutritive value such as antioxidants, phenolic compounds, dietary fibers, etc., which are also essential for nutrition (1).

According to the American Council on Science and Health, "Functional foods can be considered to be those whole, fortified, enriched, or enhanced foods that provide health benefits beyond the provision of essential nutrients (for example, vitamins and minerals), when they are consumed at efficacious levels as part of a varied diet on a regular basis" (2). Studies have been carried out on the addition of antioxidant, phenolic substance, and fiber-rich components to ice cream for functional ice cream production. Çam et al. (3) fortified ice creams with pomegranate peel extract to increase the antioxidant and phenolic content, however, they have reached a product that was sensorially unexpected. Sagdic et al. (4) increased the antioxidant and phenolic content of ice cream by the addition of grape seed extract and Karaman et al. (5) have added persimmon puree for the same purpose. Soukoulis et al. (6) fortified ice cream with apple fiber and have also reached an ice cream with enhanced viscosity. These studies have shown that the addition of fruits and vegetables give ice cream functional properties that increase its health benefits, while at the same time, a more successful product can be obtained in terms of sensory and textural properties. Some researchers have reported that adding fruits and vegetables to ice cream can either increase or decrease the amount of minerals (7–9).

Cucurbita is the genus name of a wide group of vegetables containing gourds, melon, and pumpkin. It is mostly harvested in China (7.5 Mtonnes), India (5.1 Mtonnes), Russia (1.2 Mtonnes), and the USA (1.1 Mtonnes) (10). *Cucurbita moschata* and *Cucurbita maxima* are the pumpkin types rich in carotenoids, as well as minerals, vitamins, and dietary fiber (11). In recent years, besides the studies on the quality and yield of pumpkin (12–14), the effects as a food additive have also been investigated (15–17). In these studies, it has been suggested that pumpkin be ground into flour and added to various products such as corn flakes as a food additive. Some researchers also analyzed the effects of thermal processes on the nutritive compositions of pumpkins (18–20).

In this study, different processes (freeze-drying, boiling, and baking) were applied to the pumpkins - *Cucurbita moschata* and *Cucurbita maxima*, and the pumpkins were added to the ice cream mixture. The effects of pumpkin on the physical, chemical, sensory, and textural properties of ice cream were determined. The fiber-rich ice creams were illustrated using the scanning electron microscope (SEM) to explore the effects of processing treatments. The results revealed the effects of processing steps, concentration, and the genus type species of pumpkins on ice cream structure.

MATERIALS AND METHODS

Materials

Whole milk powder (26% fat) was obtained from Milkon Dairy and Food Products Industry (Sakarya, Turkey). UHT milk (3% fat and 3% protein), kaymak (dairy cream with 65% fat, 0.8% protein), egg, sugar, and salep (as a stabilizer) were purchased from supermarkets in Sakarya. A 30 kilograms of *Cucurbita moschata* (11.4% dry matter) and *Cucurbita maxima* (8.0% dry matter) were obtained from local producers in Sakarya. Before the processing, peel, and seeds were separated, the flesh of pumpkins was cut into 1 cm^3 small cubes and then separated into 3 groups for different processing treatments (1- freeze-drying, 2- boiling, 3- baking). Raw consumed pumpkin group (R) was freeze-dried in Labconco Freezone 6 (Kansas, MO) at -45°C 0.045 mbar conditions and then blended. It was used as powder. For the boiled group (Bo), water was added in 1:1 (w:w) quantity, then boiled on a hot plate at 350 °C for 90 minutes and blended. It was used as puree. Baked pumpkin (Ba) was heated in the oven to 150 °C for 60 minutes and blended. It was also used as puree. The processed pumpkins were frozen until further use.

Preparation of Ice Cream Mix and Pumpkin Ice Creams

The ice cream mix was prepared according to the formulation; (w/w) 3.1% whole milk powder, 69.6% UHT milk, 4.3% whole egg, 9.9% kaymak (milk cream with 65% fat), 12.7% sugar, 0.4% salep. Production was carried out with some modifications on the method of Karaman et al. (5). First, milk powder and milk were blended for 2 minutes. Salep was mixed with sugar in another vessel. All of the ingredients in the mix formulation were mixed and pasteurized by indirect heating in a salep cooking machine (Remta CS3, Turkey) at 70 °C for 20 minutes, then cooled and matured at 4 °C for 48 hours.

All ice cream formulations were determined by preliminary sensory testing. The forms and concentrations of pumpkins *Cucurbita moschata* and *Cucurbita maxima* added to the ice cream mix were detailed in Table 1. Ice creams were frozen using a household ice cream machine (SIMAC GC6000 II Gelataio, Treviso, Italy). Ice creams were filled into 250 mL plastic containers for subsequent analyses and kept at -38 °C. The total formulation of ice creams is given in Table 1.

Table 1: The formulations of ice creams.

Group name	Type of pumpkin added	Properties of pumpkin	Concentration of pumpkin
NC *	None	None	None
PA-R3	A **	Raw, dried	3 %
PB-R3	B **	Raw, dried	3 %
PA-R4	A	Raw, dried	4 %
PB-R4	B	Raw, dried	4 %
PA-Bo5	A	Boiled	5 %
PB-Bo5	B	Boiled	5 %
PA-Bo10	A	Boiled	10 %
PB-Bo10	B	Boiled	10 %
PA-Ba5	A	Baked	5 %
PB-Ba5	B	Baked	5 %
PA-Ba10	A	Baked	10 %
PB-Ba10	B	Baked	10 %

* "NC" refers to the (Negative) Control sample
** "A" type of pumpkin refers to *Cucurbita moschata* and "B" type of pumpkin refers to *Cucurbita maxima*

Methods

General composition of ice cream mix
The total dry matter, fat, and protein percentage of ice cream mix were determined using a FOSS FoodScan (FoodScan Lab, Denmark) and the ash content was determined according to the method suggested by Turkish Standard Institute (21).

Total dietary fiber of pumpkins
The total dietary fiber (TDF) AACC 32-05 method was followed (22). According to the method, samples gelatinized with α-amylase were treated with protease and amyloglucosidase to remove protein and starch. Soluble dietary fiber is precipitated with ethanol. The residue is filtered; washed sequentially with 78% ethanol, 95% ethanol, and acetone; dried, and weighed. The ash correction is made, and the result is calculated as suggested in the method.

Total phenolic contents and antioxidant capacities of pumpkins
The raw pumpkins were analyzed before freeze-drying process, and the other pumpkin groups were analyzed after boiling or baking processes for their antioxidant and total phenolic contents. The extraction of antioxidants and total phenolic compounds was performed by the procedure of Wojdyło et al. (23) with a few modifications. Pumpkin (3 g) was weighed into a test tube; 10 mL of 70% aqueous methanol was added, and homogenized. Tubes were sonicated for 15 min at room temperature (20 °C). The extract was centrifuged for 10 min (1250 *g*, 4 °C), and supernatants were used for the measurements of antioxidant capacity defined as 2,2-diphenyl-1-picrylhydrazyl (DPPH) scavenging activity and total phenolic content expressed as mg of gallic acid equivalents (GAE) per 100 g dry weight.

The DPPH radical-scavenging activity was determined using the method described previously (24). For a DPPH stock solution, DPPH (5 µg) was dissolved in 70% methanol (250 ml). The stock solution was prepared fresh daily. The DPPH solution (3 mL) was added to 200 µL of extracts. The mixture was shaken and allowed to stand at room temperature in the dark for 30 minutes, and the resulting color was measured spectrophotometrically at 517 nm against blank. Methanol was used for blank measurement. The percent of DPPH discoloration of the sample was calculated according to the equation:% discoloration = $[1 - (A_{sample}/A_{control})] \times 100$.

Total phenolic content was measured using Folin-Ciocalteu colorimetric method described previously (25). Sample extracts prepared for total phenolic content (100 µL) were mixed with 0.2 mL of Folin-Ciocalteu reagent and 2 mL of H_2O, and incubated at room temperature for 3 min. Following the addition of 1 mL of 20% sodium carbonate to the mixture, total polyphenols were determined after 1 h of incubation in the dark at room temperature. The absorbance of the resulting blue color was measured at 765 nm with a spectrophotometer (Shimadzu UV–1240). Quantification was done with respect to the standard curve of gallic acid.

Determination of mineral compositions of pumpkins
The processed pumpkins were freeze-dried before the analysis. The determination of mineral composition and contents were carried out according to the method described by Ayar et al. (26); whereby 1.0 g of sample was weighed into the Teflon vessel, mixed with 5 mL of HNO_3 (65%, Sigma) and 2 mL of H_2O_2 (30%, Sigma); then digested by microwave irradiation in steps, increasing power from 250 to 650 W by 5 min increments. Mineral contents were determined by inductively coupled plasma atomic emission spectrometry (ICP-AES) (VARIAN-CCD Simultaneous ICP-AES, Australia).

Physicochemical analyses
The total dry matter (DM) and ash contents of processed pumpkins were determined before use according to AOAC methods 930.04 and 930.05 (27), respectively. Ice cream analyses were carried out, in triplicate, on the first week of storage. The titratable acidity was determined in ice creams according to AOAC 937.05 (27) and expressed as a percentage of lactic acid (LA %). The pH values of ice creams (4 °C) were measured with a pH meter (Mettler Toledo SevenCompact S220). The color of ice creams was monitored by a tintometer (Lovibond RT300, Salisbury, UK) in terms of *L*, a*, b** and the results were given as ΔE in terms of the color differences from the NK (negative control) ice cream sample.

Rheological analyses of ice creams
Overrun capacities of ice creams were determined by the comparison of the weight of ice cream mix and the final product (28). For testing rheological analyses, ice cream samples were transferred from the -38 °C freezer to a -18 °C freezer and held for a night. Before the viscosity analysis, samples were taken to a 4 °C refrigerator and held for 4 hours prior to testing. Viscosity measurements have been taken by Brookfield Viscometer RV-II

(Brookfield Engineering Laboratories, MA, USA) at 4 °C with spindle no. 7, at 100 pm on 40th second of shearing, and the results were given in terms of Poise (P). Firmness analyses of ice cream samples were carried out using a Brookfield CT3 texture analyzer (Brookfield Engineering Laboratories, MA, USA) fitted with a cylindrical probe TA 4/1000. Penetration depth was 10 mm, and penetration speed was 2 mm/s. Results were given in grams.

Sensory analyses of ice creams
Fifteen panelists working at Sakarya University were chosen for the assessment of the sensory characteristics of ice cream samples. Sensory attributes were scored in a 9-point hedonic scale test. The scoring was as follows: gumminess (1-2: none, 3-4: very little, 5-6: little, 7-9: expected as normally), icy structure (1-2: none, 3-4: very little, 5-6: little, 7-9: distinctive), appearance and melting in mouth (1-2: very bad, 3-4: bad, 5-7: good, 8-9: very good), texture, flavor, and general acceptance (1-2: weak, 3-4: moderate, 5-7: good, 8-9: very good).

Microstructure of ice creams
The ice cream samples were freeze-dried before the analysis. The microstructure of dried ice creams was visualized using an FEI Quanta FEG 250 (FEI Corporate, Hillsboro, OR, USA) field emission scanning electron microscope (FE-SEM) with an LFD detector. Images were obtained at 2 kV and recorded at 2000 – 16,000 magnifications. The best results were taken in 2000 magnifications.

Statistical analysis
The data obtained from the physicochemical, rheological, and sensory analyses and comparisons were statistically evaluated by one-way ANOVA followed by Tukey's test using SPSS Statistics 20.0.0 (SPSS Inc., Chicago, IL, USA). Values of $P < 0.05$ were regarded as statistically significant.

RESULTS AND DISCUSSION

The general composition of ice cream mix
The average composition of the ice cream mix was determined as: 41.3% dry matter, 10.0% fat, 5.4% protein, and 0.96% ash. The results were in accordance to the literature data (29,30) except for the fat content. Fat ratios vary according to the amount of cream added and the last products are labelled with different names depending on the fat content according to the Regulations (31). Our product can be labelled as "whole fat Maraş style ice cream" according to its fat and salep content.

Some chemical and compositional characteristics of processed pumpkins
The DM, ash, DPPH scavenging activity, total phenolic compounds, and TDF contents of processed pumpkins are given in Table 2, and the mineral compositions are shown in Table 3. According to the statistical analysis, the DM of the pumpkins differed according to the pumpkin variety and the process. The ash content differed independently from the variety and the process.

According to Table 2, the antioxidant capacity of *Cucurbita moschata* in terms of DPPH scavenging activity decreased with boiling and baking. In contrast, reverse baking caused an increase in the antioxidant content of *Cucurbita maxima*. According to the results of Dini et al. (32), cooking had increased the DPPH scavenging activity of pumpkin due to the production of redox-active secondary metabolites or breakdown compounds. However, Azizah et al. (33) also demonstrated the effect of boiling time in a decrease of the antioxidant activity, with a study of boiling the pumpkin from 2 minutes to 6 minutes. DPPH scavenging activity also is highly affected from the variety, from the region, from the parts of the pumpkin and from the maturity of the pumpkin (15,34).

The total phenolic content of *Cucurbita moschata* was considerably higher than the *Cucurbita maxima*. However, although its higher phenolic content, *Cucurbita moschata* samples were affected from heat treatment (boiling and baking) (Table 2). As a result, it can be concluded that *Cucurbita maxima* contains lower phenolic substances, but these phenolics are more resistant to thermal processes. Considering the effect of thermal processing on total phenolics, there are both studies showing the phenolics increase and decrease by heat treatment (32,33). On the other hand, freeze-drying has no effect on total phenol according to the results of the study done by Dirim and Çalışkan (35). Hussain et al. (36) also analyzed *Cucurbita maxima* and found the total phenolic content as 135 mg GEA / 100 g flesh fruit powder, close to our results. Kulczyński et al. (37) analyzed different varieties of *Cucurbita moschata* and the results have ranged from 47-101 mg GEA / 100 g DM.

The TDF content changed depending on the pumpkin variety. However, as expected, it was affected from neither boiling nor baking due to mass balance. TDF is a vital source for intestinal health, and it is a carrier for antioxidants, mainly polyphenolic compounds, as well (38). It is also a functional agent having fat-binding, gel-forming, chelating and texturizing properties (39). TDF content in the flesh of *Cucurbita moschata* and *Cucurbita maxima* were measured as 24.5% and 31.1%, respectively, in our study. However, lower TDF contents were determined respectively as 7.4% and 10.9% in another study (40).

Table 2: The properties of processed pumpkins.

Group name	DM (%)	Ash (%)	DPPH scavenging activity (%)	Total phenolic compds (mg GAE / 100 g DM)	TDF (%)
PA-R	11.4 ± 0.2 c	0.35 ± 0.02 bc	26.2 ± 1.2 a	237.5 ± 1.0 a	24.5 ± 0.1 b
PB-R	8.0 ± 0.3 e	0.48 ± 0.02 b	9.0 ± 0.1 c	123.9 ± 3.7 c	31.1 ± 0.2 a
PA-Bo	10.7 ± 0.1 c	0.31 ± 0.01 c	16.6 ± 1.4 b	192.1 ± 2.1 b	23.6 ± 0.1 b
PB-Bo	9.0 ± 0.0 d	0.42 ± 0.00 bc	9.9 ± 0.2 c	119.2 ± 1.4 c	30.5 ± 0.3 a
PA-Ba	18.1 ± 0.0 a	0.45 ± 0.03 bc	14.8 ± 0.1 b	208.0 ± 5.0 b	24.3 ± 0.2 b
PB-Ba	17.1 ± 0.2 b	0.83 ± 0.06 a	16.7 ± 0.3 b	130.9 ± 4.7 c	31.3 ± 0.0 a

PA : *Cucurbita moschata*, PB : *Cucurbita maxima* ; R : Raw, Bo : Boiled, Ba : Baked

According to Table 3, K content was pumpkin variety dependent; however, the other analyzed minerals Ca, Mg, Mn, Na, and P were not affected by variety. The Ca and K contents of *Cucurbita maxima* decreased significantly by boiling or baking. However, no change was observed in *Cucurbita moschata*. *Cucurbita maxima* was more heat stable than *Cucurbita moschata* according to their phenolic content in Table 2, but the opposite was observed when their Ca and K contents in Table 3 were evaluated. Zn content revealed an increase by boiling process in *Cucurbita moschata* pumpkin variety. The increase can be explained by possible contamination from the distilled water used for boiling (41). In a study from literature, Ca, K, Mg, Mn, Na, P, and Zn contents of *Cucurbita maxima* from Colombia were measured respectively as 2400, 33467, 1733, 1.33, 333, 3400, and 12.0 mg / kg DM (42). In this study, Ca, Mg and Mn contents were lower than our study, while K, Na, P and Zn contents were higher. K represented the main mineral with the highest content in both our study and Leterme et al. (42).

Table 3: Mineral composition of processed pumpkins (mg / kg DM).

Group name	Calcium (Ca)	Potassium (K)	Magnesium (Mg)	Manganese (Mn)	Sodium (Na)	Phospho-rus (P)	Zinc (Zn)
PA-R	3830 ± 160 ab	9860 ± 216 c	973 ± 37 a	4.81 ± 0.25 a	472 ± 61 a	2161 ± 119 a	11.2 ± 0.3 ab
PB-R	4652 ± 166 a	18725 ± 148 a	1115 ± 53 a	4.60 ± 0.04 a	450 ± 43 a	2158 ± 112 a	10.6 ± 0.6 b
PA-Bo	3797 ± 116 ab	9925 ± 192 c	937 ± 33 a	4.68 ± 0.33 a	417 ± 34 a	2114 ± 160 a	13.6 ± 0.2 a
PB-Bo	3760 ± 154 b	16950 ± 171 b	1106 ± 56 a	4.65 ± 0.43 a	428 ± 41 a	2186 ± 93 a	11.4 ± 0.5 ab
PA-Ba	3785 ± 173 ab	9754 ± 182 c	937 ± 38 a	4.66 ± 0.22 a	383 ± 34 a	2021 ± 123 a	11.5 ± 0.1 ab

PB-Ba	3729 ± 155 b	16165 ± 133 b	1041 ± 54 a	4.64 ± 0.15 a	392 ± 45 a	2195 ± 69 a	10.0 ± 0.6 b

PA : *Cucurbita moschata*, PB : *Cucurbita maxima* ; R : Raw, Bo : Boiled, Ba : Baked

pH, Acidity, and Color Properties of Ice Cream Samples

The pH, acidity, and color properties of ice creams are given in Table 4. According to the literature, while the pH of raw vegetables can be increased by heat treatment, pH decreases as the heat treatment load increases (43). In our study, it was determined that the pH of the products with the addition of baked pumpkin was significantly lower. ($P < 0.05$). Color properties differed irregularly in all samples. However, when the results are taken into account, some inferences can be made; *Cucurbita maxima*-based ice creams more different than the *Cucurbita moschata*. The concentration of the pumpkins was an important factor on color. Raw pumpkins affected the color more than processed pumpkins, because of their high concentrations in powder form. Another finding was that the effect of baking on the color was greater than that of boiling. In a study in the literature, color of ice creams fortified with peach fibers exhibited identical changes with varying peach fiber contents (44). Guiné and Barroca (45) stated that freeze-drying led to a more pronounced lightening (higher L values) and less green discoloration (lower Δb) of *Cucurbita maxima*.

Table 4: pH, acidity and color properties of ice cream samples.

Group name	pH	Acidity (% LA)	Color (ΔE)	Overrun (%)	Firmness (g)	Viscosity (P)
NC	6.66 ± 0.01 ab	0.34 ± 0.01 b	0.0 ± 0.0 i	26.7 ± 0.3 a	48.5 ± 0.9 h	56.8 ± 1.6 g
PA-R3	6.68 ± 0.01 a	0.43 ± 0.01 a	26.7 ± 0.3 c	22.2 ± 0.1 abc	82.8 ± 3.5 ef	91.7 ± 1.3 de
PB-R3	6.64 ±0.00 b	0.40 ± 0.00 a	31.2 ± 0.2 b	18.8 ± 0.6 abc	103.3 ± 2.9 cd	125.3 ± 0.5 c
PA-R4	6.68 ± 0.02 a	0.44 ± 0.00 a	26.5 ± 0.2 c	20.9 ± 0.1 abc	126.0 ± 4.2 b	142.5 ± 1.1 b
PB-R4	6.64 ± 0.01 b	0.42 ± 0.02 a	38.6 ± 0.6 a	14.9 ± 0.2 c	116.7 ± 6.4 bc	135.0 ± 0.6 b
PA-Bo5	6.65 ± 0.00 b	0.32 ± 0.01 b	5.4 ± 0.4 h	23.1 ± 4.2 abc	57.3 ± 0.8 gh	74.0 ± 2.2 f
PB-Bo5	6.65 ± 0.01 b	0.31 ± 0.03 b	5.7 ± 0.1 gh	18.3 ± 1.2 abc	90.0 ± 5.4 de	119.5 ± 3.9 c
PA-Bo10	6.65 ± 0.00 b	0.30 ± 0.00 b	8.1 ± 0.2 f	21.3 ± 4.5 abc	89.5 ± 3.5 de	90.1 ± 0.4 e
PB-Bo10	6.64 ± 0.00 b	0.30 ± 0.00 b	10.1 ± 0.4 e	15.4 ± 0.2 bc	146.3 ± 3.2 a	175.0 ± 1.8 a
PA-Ba5	6.59 ± 0.00 c	0.31 ± 0.00 b	6.8 ± 0.2 g	26.1 ± 0.1 ab	70.2 ± 1.3 fg	72.3 ± 0.7 f
PB-Ba5	6.58 ± 0.02	0.29 ± 0.01	11.0 ± 0.6	22.9 ± 1.3	65.8 ± 2.0	88.4 ± 1.3

	c	b	e	abc	fgh	e
PA-Ba10	6.59 ± 0.01 c	0.32 ± 0.03 b	10.2 ± 0.2 e	21.0 ± 0.3 abc	68.8 ± 1.8 fg	91.2 ± 0.3 e
PB-Ba10	6.58 ± 0.00 c	0.30 ± 0.00 b	15.1 ± 0.6 d	19.2 ± 2.6 abc	83.0 ± 1.7 ef	100.3 ± 0.1 d

NC : Negative control PA : *Cucurbita moschata*, PB : *Cucurbita maxima* ; R : Raw, Bo : Boiled, Ba : Baked

Rheological Properties of Ice Cream Samples

The rheological properties of ice cream samples are given in Table 4. The addition of pumpkin reduced the overrun capacity. *Cucurbita maxima* added ice creams revealed a lower overrun capacity than *Cucurbita moschata* added ones. Increasing pumpkin concentrations caused an increase in firmness and viscosity values of ice creams. The rheological effect of pumpkin on ice cream was also confirmed by Kulkarni et al. (46). While the firmness value was 48.5 g in the negative control sample, the addition of pumpkin increased the value and with a 146.3 g measurement, the ice cream containing boiled *Cucurbita maxima* had the highest firmness value among the groups. Viscosity results also correlated with hardness. The viscosity of the product with the highest hardness was measured as 175.0 P, and the viscosity value in the control sample was found to be relatively low (56.8 P).

In addition, while the DM of *Cucurbita maxima* was lower, higher firmness and viscosity were measured in *Cucurbita maxima* added groups compared to *Cucurbita moschata* added ones. If the rheological properties of ice creams are summarized, the overrun capacity was not statistically affected by pumpkin addition (except for the PB-R4 sample); however, firmness and viscosity characteristics were improved by increasing pumpkin concentrations.

Sensory Attributes of Ice Cream Samples

The sensory scores of ice cream samples are given in Table 5. According to the panelists, the addition of pumpkin slightly affected the melting properties of ice cream but did not cause any change in other sensory properties. These sensory results are promising in terms of incorporation of pumpkin into ice cream. Most of them have scored 7 and above, except for icy structure. Icy structure is a texture defect in ice creams, and 1-3 points for icy structure evaluation is desired in an ice cream. These scores revealed that ice cream formulation and processing was available according to its textural quality and the addition of pumpkin did not cause any icy texture. Karaman et al. (47) stated that the persimmon puree addition decreased the taste scores and general acceptance of the ice creams. Çam et al. (3) stated that the product to which they added pomegranate peel extract caused astringency and an unnatural taste. In a study that added soluble soybean polysaccharides to ice cream as a fiber source, the flavor and sweetness intensity decreased, and an adverse effect on the texture was observed (48).

The Microstructure of Ice Cream Samples

The microstructures of pumpkin-added ice creams are shown in Figure 1 with the magnification of 2000 x. Samples presented porous structures. The application of freeze drying in ice creams caused air gaps. According to our results and literature knowledge (49), it is observed that, air gaps are also significantly affected by the formulation of the product.

It was observed that the fibrous image was mostly lost by boiling. The boiled pumpkin added samples (Bo) were featured closest to the control sample (NC). Especially in the PB-Ba10 sample, the structure of fibers and bridges was obtained clearly.

Table 5: The sensory properties of ice creams.

Group name	Appearance	Gumminess	Icy structure	Melting in the mouth	Texture	Flavor	General acceptance
NC	7.8 ± 1.3 a	7.8 ± 1.1 a	1.3 ± 0.6 a	8.8 ± 0.5 ab	8.8 ± 0.5 a	7.5 ± 1.3 a	7.5 ± 1.4 a
PA-R3	6.8 ± 1.1 a	7.8 ± 1.1 a	1.7 ± 0.6 a	8.3 ± 1.0 ab	7.3 ± 2.2 a	6.8 ± 2.6 a	7.2 ± 1.3 a
PB-R3	7.4 ± 1.1 a	7.2 ± 1.1 a	3.3 ± 1.5 a	7.3 ± 0.5 bc	6.8 ± 1.9 a	7.3 ± 2.1 a	7.8 ± 1.2 a
PA-R4	7.0 ± 1.0 a	7.4 ± 1.5 a	2.0 ± 1.0 a	6.5 ± 1.0 c	7.0 ± 0.8 a	7.3 ± 1.0 a	6.5 ± 1.9 a
PB-R4	6.6 ± 1.1 a	7.6 ± 1.1 a	2.7 ± 2.1 a	7.3 ± 1.0 bc	6.3 ± 1.5 a	7.3 ± 0.5 a	6.5 ± 1.4 a
PA-Bo5	8.2 ± 1.1 a	8.0 ± 1.0 a	1.3 ± 0.6 a	8.3 ± 0.5 ab	8.0 ± 0.8 a	7.3 ± 1.0 a	6.5 ± 1.8 a
PB-Bo5	8.0 ± 1.2 a	8.2 ± 1.3 a	1.3 ± 0.6 a	8.0 ± 0.8 abc	8.0 ± 0.8 a	6.3 ± 2.4 a	6.8 ± 1.5 a
PA-Bo10	8.0 ± 1.0 a	7.0 ± 1.4 a	1.3 ± 0.6 a	8.5 ± 0.6 ab	7.8 ± 1.0 a	5.5 ± 1.7 a	5.8 ± 1.8 a
PB-Bo10	7.6 ± 0.9 a	6.0 ± 1.4 a	1.3 ± 0.6 a	8.8 ± 0.5 ab	6.5 ± 1.9 a	5.3 ± 1.7 a	6.0 ± 1.4 a
PA-Ba5	7.6 ± 1.5 a	7.4 ± 1.1 a	1.3 ± 0.6 a	9.0 ± 0.0 a	8.0 ± 0.8 a	6.8 ± 2.1 a	6.7 ± 1.6 a
PB-Ba5	8.0 ± 1.4 a	6.8 ± 1.3 a	1.3 ± 0.6 a	8.8 ± 0.5 ab	8.0 ± 0.8 a	6.5 ± 1.3 a	67.2 ± 1.5 a
PA-Ba10	7.4 ± 2.1 a	7.4 ± 0.9 a	1.3 ± 0.6 a	8.5 ± 0.6 ab	8.0 ± 0.8 a	6.3 ± 2.2 a	6.5 ± 1.4 a
PB-Ba10	8.0 ± 1.4 a	7.2 ± 1.1 a	1.3 ± 0.6 a	8.5 ± 0.6 ab	8.0 ± 0.8 a	7.0 ± 1.4 a	7.2 ± 1.2 a

NC : Negative control PA : *Cucurbita moschata*, PB : *Cucurbita maxima* ; R : Raw, Bo : Boiled, Ba : Baked

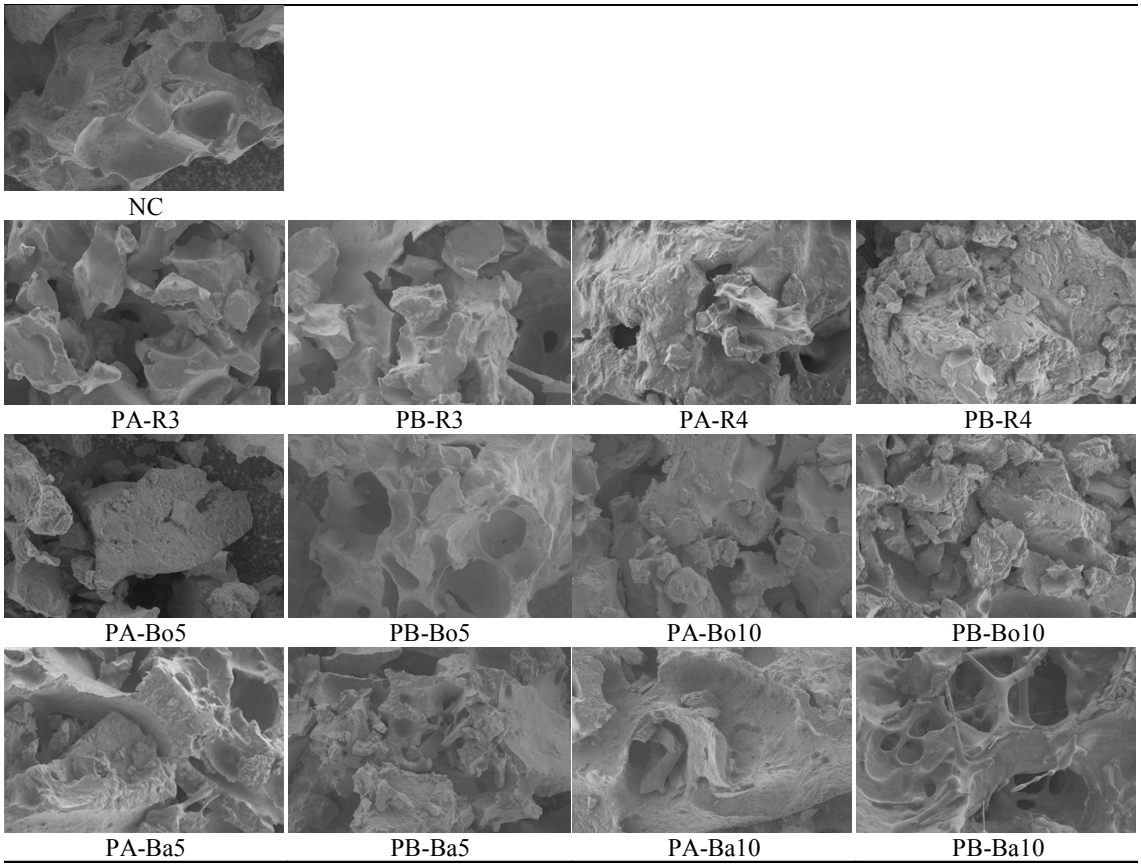

NC : Negative control PA : *Cucurbita moschata*, PB : *Cucurbita maxima* ; R : Raw, Bo : Boiled, Ba : Baked

Figure 1: The microstructures of ice creams (FE-SEM x 2000).

CONCLUSIONS

As a conclusion of our study, pumpkin addition to ice cream is a sensorially acceptable application. Processing steps of boiling and baking decreased some health-promoting effects (DPPH scavenging capacity and total phenolic content), while some of them revealed the same (TDF content and mineral composition). Fortification with pumpkin did not cause a significant decrease in the overrun but improved the firmness considerably. The baking process did not reveal a change in TDF content but screened a higher fiber image. There were also some differences according to the variety of the pumpkins. Comparison all the data with NC samples, it can be revealed that pumpkin addition achieved health-promoting compounds to the ice cream without any adverse effect on its quality properties.

FUNDING

This study was funded by the Scientific Research Projects Unit of Sakarya University (grant number 2016-01-16-020).

CONFLICT OF INTEREST

The authors declare that they have no conflict of interest.

REFERENCES

1. Soukoulis C, Fisk ID, Bohn T. Ice Cream as a Vehicle for Incorporating Health-Promoting Ingredients: Conceptualization and Overview of Quality and Storage Stability: Functional ice cream…. Comprehensive Reviews in Food Science and Food Safety. 2014 Jul;13(4):627–55. <DOI>.

2. Hasler CM. Functional Foods: Benefits, Concerns and Challenges—A Position Paper from the American Council on Science and Health. The Journal of Nutrition. 2002 Dec 1;132(12):3772–81. <DOI>.

3. Çam M, Erdoğan F, Aslan D, Dinç M. Enrichment of Functional Properties of Ice Cream with Pomegranate By-products: Enrichment of ice cream…. Journal of Food Science. 2013 Oct;78(10):C1543–50. <DOI>.

4. Sagdic O, Ozturk I, Cankurt H, Tornuk F. Interaction Between Some Phenolic Compounds and Probiotic Bacterium in Functional Ice Cream Production. Food Bioprocess Technol. 2012 Nov;5(8):2964–71. <DOI>.

5. Karaman S, Toker ÖS, Yüksel F, Çam M, Kayacier A, Dogan M. Physicochemical, bioactive, and sensory properties of persimmon-based ice cream: Technique for

order preference by similarity to ideal solution to determine optimum concentration. Journal of Dairy Science. 2014 Jan;97(1):97–110. <DOI>.

6. Soukoulis C, Lebesi D, Tzia C. Enrichment of ice cream with dietary fibre: Effects on rheological properties, ice crystallisation and glass transition phenomena. Food Chemistry. 2009 Jul;115(2):665–71. <DOI>.

7. Soukoulis C, Tzia C. Response surface mapping of the sensory characteristics and acceptability of chocolate ice cream containing alternate sweetening agents. Journal of Sensory Studies. 2010 Feb;25(1):50–75. <DOI>.

8. Erkaya T, Dağdemir E, Şengül M. Influence of Cape gooseberry (Physalis peruviana L.) addition on the chemical and sensory characteristics and mineral concentrations of ice cream. Food Research International. 2012 Jan;45(1):331–5. <DOI>.

9. Dagdemir E. Effect of vegetable marrow (Cucurbita pepo L.) on ice cream quality and nutritive value. Asian Journal of Chemistry. 2011;23(10):4684–8.

10. Food and Drug Administration [Internet]. Food and Drug Administration. 2020 [cited 2022 Apr 11]. <URL>.

11. de Escalada Pla MF, Ponce NM, Stortz CA, Gerschenson LN, Rojas AM. Composition and functional properties of enriched fiber products obtained from pumpkin (Cucurbita moschata Duchesne ex Poiret). LWT - Food Science and Technology. 2007 Sep;40(7):1176–85. <DOI>.

12. Nagar A, Sureja AK, Kumar S, Munshi A, Gopalakrishnan S, Bhardwaj R. Genetic Variability and Principal Component Analysis for Yield and its Attributing Traits in Pumpkin (Cucurbita moschata Duchesne Ex Poir.). Soc Plant Res. 2017;133:81.

13. Tamilselvi A. Line x Tester analysis for yield and its component traits in pumpkin (Cucurbita moschata Duch.Ex Poir). El J Plant Breeed. 2015;6(4):1004–10. <URL>.

14. Rana M, Rasu M, Islam A, Hossain M. Diallel Analysis of Quality and Yield Contributing Traits of Pumpkin (Cucurbita moschata Duch. ex Poir.). Agricult. 2016;14(1):15–32. <URL>.

15. Kulaitienė J, Jarienė E, Danilčenko H, Černiauskienė J, Wawrzyniak A, Hamulka J, et al. Chemical composition of pumpkin (Cucurbita maxima D.) flesh flours used for food. Journal of Food, Agriculture & Environment. 2014;12(3 & 4):61–4.

16. Peksa A, Kita A, Jariene E, Danilcenko H, Gryszkin A, Figiel A, et al. Amino Acid Improving and Physical Qualities of Extruded Corn Snacks Using Flours Made from Jerusalem Artichoke (Helianthus tuberosus), Amaranth (Amaranthus cruentus L.) and Pumpkin (Cucurbita maxima L.): Amino acid improving and physical qualities of extruded corn snacks. Journal of Food Quality. 2016 Dec;39(6):580–9. <DOI>.

17. Yin L, Wang C. Morphological, thermal and physicochemical properties of starches from squash (Cucurbita maxima) and pumpkin (Cucurbita moschata). Journal of Horticulture. 2016;3(04):187.

18. Que F, Mao L, Fang X, Wu T. Comparison of hot air-drying and freeze-drying on the physicochemical properties and antioxidant activities of pumpkin (Cucurbita moschata Duch.) flours. Int J Food Sci Tech. 2008 Jul;43(7):1195–201. <DOI>.

19. Guiné RPF, Pinho S, Barroca MJ. Study of the convective drying of pumpkin (Cucurbita maxima). Food and Bioproducts Processing. 2011 Oct;89(4):422–8. <DOI>.

20. Mendelova A, Mendel L, Fikselová M, Mareček J, Vollmannová A. Winter squash (Cucurbita moschata Duch) fruit as a source of biologically active components after its thermal treatment. Potravinárstvo: Slovak Journal of Food Sciences. 2017;11(1):489–95.

21. ICS 67.100.10) Süt ve İşlem Görmüş Süt Ürünleri Standardı - İnek Sütü, Çiğ. Ankara, Turkey: Türk Standartları Enstitüsü; 2002. Report No.: TS 1018.

22. American Association of Cereal Chemists. Approved Methods Committee. Approved methods of the American association of cereal chemists. Vol. 1. Amer Assn of Cereal Chemists; 2000. ISBN: 1-891127-12-8.

23. Wojdylo A, Oszmianski J, Czemerys R. Antioxidant activity and phenolic compounds in 32 selected herbs. Food Chemistry. 2007;105(3):940–9. <DOI>.

24. Brand-Williams W, Cuvelier ME, Berset C. Use of a free radical method to evaluate antioxidant activity. LWT - Food Science and Technology. 1995;28(1):25–30. <DOI>.

25. Singleton VL, Rossi JA. Colorimetry of Total Phenolics with Phosphomolybdic-Phosphotungstic Acid Reagents. American Journal of Enology and Viticulture. 1965;16(3):144–58. <URL>.

26. Ayar A, Sert D, Akın N. The trace metal levels in milk and dairy products consumed in middle Anatolia—Turkey. Environ Monit Assess. 2009 May;152(1–4):1–12. <DOI>.

27. AOAC. Official methods of analysis of AOAC International. Gaithersburg, MD, USA: AOAC; 2000.

28. Marshall RT, Goff HD, Hartel RW, SpringerLink (Online service). Ice Cream. 2003. ISBN: 978-0-306-47700-3.

29. Hatipoğlu A, Türkoğlu H. A research on the quality features of ice cream produced using some fat substitutes. Journal of Food Science and Engineering. 2020;10:1–10.

30. Fedakar F, Turgay Ö. Maraş Dondurmasının Bazı Özelliklerinin İncelenmesi. Gıda ve Yem Bilimi Teknolojisi Dergisi. 2020 Feb 7;(23):19–24. <URL>.

31. Türk Gıda Kodeksi Dondurma Tebliği. Tarım ve Köy İşleri Bakanlığı; 2005 Jan. Report No.: 2004/45.

32. Dini I, Tenore GC, Dini A. Effect of industrial and domestic processing on antioxidant properties of pumpkin pulp. LWT - Food Science and Technology. 2013 Sep;53(1):382–5. <DOI>.

33. Azizah A, Wee K, Azizah O, Azizah M. Effect of boiling and stir frying on total phenolics, carotenoids and radical scavenging activity of pumpkin (Cucurbita moschato). International Food Research Journal. 2009;16(1):45–51.

34. Jacobo-Valenzuela N, Zazueta-Morales J de J, Gallegos-Infante JA, Aguilar-Gutierrez F, Camacho-

Hernandez IL, Rocha-Guzman NE, et al. Chemical and Physicochemical Characterization of Winter Squash (Cucurbita moschata D.). Not Bot Hort Agrobot Cluj. 2011 May 30;39(1):34. <DOI>.

35. Dirim SN, Çalıskan G. Determination of the effect of freeze drying process on the production of pumpkin (Cucurbita moschata) puree powder and the powder properties. J Food. 2012;37:203–10.

36. Hussain A, Kausar T, Din A, Murtaza MA, Jamil MA, Noreen S, et al. Determination of total phenolic, flavonoid, carotenoid, and mineral contents in peel, flesh, and seeds of pumpkin (Cucurbita maxima). J Food Process Preserv [Internet]. 2021 Jun [cited 2022 Apr 11];45(6). <DOI>.

37. Kulczyński B, Sidor A, Gramza-Michałowska A. Antioxidant potential of phytochemicals in pumpkin varieties belonging to Cucurbita moschata and Cucurbita pepo species. CyTA - Journal of Food. 2020 Jan 1;18(1):472–84. <DOI>.

38. Saura-Calixto F. Dietary Fiber as a Carrier of Dietary Antioxidants: An Essential Physiological Function. J Agric Food Chem. 2011 Jan 12;59(1):43–9. <DOI>.

39. Borderías AJ, Sánchez-Alonso I, Pérez-Mateos M. New applications of fibres in foods: Addition to fishery products. Trends in Food Science & Technology. 2005 Oct;16(10):458–65. <DOI>.

40. Kim MY, Kim EJ, Kim Y-N, Choi C, Lee B-H. Comparison of the chemical compositions and nutritive values of various pumpkin (Cucurbitaceae) species and parts. Nutr Res Pract. 2012 Feb;6(1):21–7. <DOI>.

41. Cornelison GL, Mihic SJ. Contaminating levels of zinc found in commonly-used labware and buffers affect glycine receptor currents. Brain Research Bulletin. 2014 Jan;100:1–5. <DOI>.

42. Leterme P, Buldgen A, Estrada F, Londoño AM. Mineral content of tropical fruits and unconventional foods of the Andes and the rain forest of Colombia. Food Chemistry. 2006 Apr;95(4):644–52. <DOI>.

43. Kim B-C, Hwang J-Y, Wu H-J, Lee S-M, Cho H-Y, Yoo Y-M, et al. Quality changes of vegetables by different cooking methods. Culinary science and hospitality research. 2012;18(1):40–53.

44. Yangılar F. Production and evaluation of mineral and nutrient contents, chemical composition, and sensory properties of ice creams fortified with laboratory-prepared peach fibre. Food & Nutrition Research. 2016 Jan;60(1):31882. <DOI>.

45. Guiné RPF, Barroca MJ. Effect of drying treatments on texture and color of vegetables (pumpkin and green pepper). Food and Bioproducts Processing. 2012 Jan;90(1):58–63. <DOI>.

46. Kulkarni AS, Joshi DC, Tagalpallewar G, Gawai KM. Development of technology for the manufacture of pumpkin ice cream. Indian J Dairy Sci. 2017;70(6):701–6.

47. Karaman S, Toker ÖS, Yüksel F, Çam M, Kayacier A, Dogan M. Physicochemical, bioactive, and sensory properties of persimmon-based ice cream: Technique for order preference by similarity to ideal solution to determine optimum concentration. Journal of Dairy Science. 2014 Jan;97(1):97–110. <DOI>.

48. Chen W, Duizer L, Corredig M, Goff HD. Addition of Soluble Soybean Polysaccharides to Dairy Products as a Source of Dietary Fiber. Journal of Food Science. 2010 Aug;75(6):C478–84. <DOI>.

49. Granger C, Langendorff V, Renouf N, Barey P, Cansell M. Short Communication: Impact of Formulation on Ice Cream Microstructures: an Oscillation Thermo-Rheometry Study. Journal of Dairy Science. 2004 Apr;87(4):810–2. <DOI>.

JOTCS B
Journal of the Turkish Chemical Society
Section: B
Chemical Engineering
TURKISH CHEMICAL SOCIETY

Synthesis and Characterization of Cu/KIT-6 Silicas for Use in CO_2 Adsorption

Gamze GÜNDÜZ MERİÇ

Engineering Faculty, Chemical Engineering Department, Bilecik Seyh Edebali University 11210 Gulumbe Bilecik/TURKEY

Abstract: KIT-6 is a mesoporous material with cubic la3d symmetry, adjustable porous 3-dimensional (3D) silica structure, advanced wall thickness, and excellent thermal/hydrothermal stability. KIT-6, with its cubic la3d symmetrical structure, has adjustable pore size. In this study, characterization studies of Cu/KIT-6 material by preparing different Si/Cu: blank, 1, 3, 5 molar ratios were performed by SEM, SEM-Mapping, TEM, XRD, N_2 adsorption-desorption, FTIR analysis. Cu-based la3d mesoporous silica KIT-6 was synthesized by hydrothermal method and different silicon to copper (Cu) ratios $n_{Si/Cu}$: 1, 3, 5, and blank KIT-6 were investigated for CO_2 adsorption capacity at ambient conditions. The highest CO_2 adsorption of 1.70 mmol CO_2/g at 0 °C and 1.2 bar was achieved for $n_{Si/Cu}$:1 ratio Cu/KIT-6. These materials are thought to be useful for the emission of CO_2 that causes global warming.

Keywords: KIT-6, silicas, mesoporous, Cu, CO_2 capture, global warming.

Submitted: February 15, 2022. **Accepted:** May 11, 2022.

Cite this: Gündüz Meriç G. Synthesis and Characterization of Cu/KIT-6 Silicas for Use in CO2 Adsorption. JOTCSB. 2022;5(1):21–8.

***Corresponding author. E-mail:** gamze.gunduz@bilecik.edu.tr. Tel: +90228 214 1765 Fax:+90228 214 1222

INTRODUCTION

The greenhouse gases contain CH_4, CO_2, N_2O, sulfur hexafluoride, and chloro-fluorocarbons (1). CO_2 is the most serious one for global warming compared to other gases (2, 3). CO_2 concentration in the atmosphere increases rapidly and affects global warming (4). Global warming is one of the major problems to an ecosystem in the world. This rapid increase also affects the environment (5-7). CO_2 concentration will reach 450 ppm in the future (8) and it causes an increase in global surface temperature (about 2 °C) (9). For controlling global warming, CO_2 capture is the main solution according to the United Nations countries (10). CO_2 capture and storage is very important to minimize its negative effects on climate change and to reduce CO_2 emission (11, 12). Solid porous adsorbents are widely used due to their large surface area and pore volume for CO_2 adsorption techniques (13). Sun et al. (14) prepared CaO-based sorbents and they found a high-temperature CO_2 capacity of 7.6 mmol/g at 377 K and they showed excellent stability over 10 cycles. Kishor et al. (15) reported 1.56 mmol CO_2/g at 30 °C for APTES-grafted KIT-6. Huang et al. (16) studied MCM-48 for CO_2 adsorption and found 98.2 mg/g at 1 atm and room temperature. Gargiulo et al. (17) measured the highest CO_2 capacity of 5.3 mol/kg at 298 K under 1 bar with NaX RHA zeolite. Yan et al. (18) prepared zeolite NaX@NaA core-shell microspheres for its high CO_2 adsorption capacity and they reported 5.60 mmol/g CO_2 at 298 K and 100 kPa total pressure. Huang et al. (19) found that 2.2 mmol CO_2/g with amine-based MCM-48 under 1 atm at 298 K. Liu et al. (20,21) studied with N-(2-aminoethyl)-3-aminopropyltrimethoxysilane-based SBA-15 and the adsorption capacity was 0.727 mmol/g under 101.325 kPa at 333 K. Hiyoshi et al. (22) prepared aminosilanes on SBA-15 adsorbents and they reported 1.8 mmol/g- adsorbent under 15 kPa at 333 K. Zhao et al. (23) studied with porous SiO_2 supported CaO and they found a 7.5 mmol CO_2/g capacity.

KIT-6 is a mesoporous SiO_2 with a la3d structure and larger pore diameter. Most researchers in recent years have paid attention to their favorable physicochemical properties that increase the metal distribution and subsequently the accessibility of the reactants (24-28). Its specific (3D) cubic channels

give it a more suitable structure for the diffusion of reactant gas (29-31). KIT-6 is a highly stable silica framework as CO_2 support (32). On the other hand, there is very little literature working on the CO_2 adsorption capacity in silica KIT-6 supplement and there are no reports on Cu-based KIT-6. SiO_2 is also a widely available sinter-resistant and cost-effective material for economical CO_2 capture. The adsorption capacity of Cu/KIT-6 was investigated by CO_2 adsorption tests and materials were characterized by BET (Brauner-Emmett-Teller) isotherms, SEM (Scanning electron microscopy), SEM-EDX (Scanning electron microscopy, energy dispersive x-ray analysis), SEM-Mapping (Analytical mapping), TEM (Transmission electron microscopy), XRD (X-ray diffraction analysis), and FT-IR (Fourier transform infrared spectroscopy) analysis.

EXPERIMENTAL SECTION

Synthesis of mesoporous silicas

Cu-based KIT-6 with different Cu contents was prepared with a typical procedure (33). Cu/KIT-6 mesoporous la3d materials containing $n_{Si/Cu}$= 1, 3, 5 and blank KIT-6 were synthesized using Pluronic P123 (Poly(ethylene glycol)-block-poly(propyleneglycol)-block-poly(ethylene glycol)-PEG-PPG-PEG (CAS no: 9003-11-6) (Carbosynth) and n-butanol ($CH_3(CH_2)_3OH$) (CAS no: 71-36-3) (Merck). 5.0 g of P123 was dissolved in 161 mL of 0.5 M Hydrochloric acid (HCl) (38%) (Cas no: 7647-01-0) (Merck) at 35°C. After dissolution was complete, 5.0 g of n-butanol was added and the resulting mixture was stirred at 35 °C for 1 hour. In order to obtain the desired Si/Cu: 1, 3, 5 molar ratio, the metal source Copper(II) chloride ($CuCl_2$) (CAS no: 7447-39-4) (Sigma-Aldrich) and the required amount of tetraethyl orthosilicate ($Si(OC_2H_5)_4$) (CAS no: 78-10-4) (TEOS) (ABCR) were added to the mixture and it was stirred for 24 hours. The reaction mixture was taken into a 250-mL Teflon autoclave for hydrothermal treatment (24 hours at 100 °C). The resulting solid was separated and dried at 100 °C overnight. The surfactant was removed by calcination in dry air at 550 °C for 5 hours.

Material characterization

The morphology of Cu-based materials was evaluated by TEM using JEOL JEM-1220 and by SEM using the Quanta 400F Field Emission device. Textural parameters (BET surface areas, total pore volume, and pore sizes) were obtained by N_2 ads.-des. isotherms. The specific surface areas of the materials were determined by the BET method at 77 K under N_2 gas adsorption. From the plot of relative pressure (P/P_0 between 0 and 1.0) versus quantity adsorbed (cm^3 /g STP) were determined. XRD patterns of the materials were obtained with a Panalytical Empyrean device at 200 kV and 50 mA with 2Θ values ranging from 5-80° and a speed of 10°/min. Prior to measurements, materials were gassed overnight at 250 °C and 100 mmHg. ATR-FT-IR spectra were obtained on a Cary 630 between 4000 and 400 cm^{-1} using diluted samples. CO_2 adsorption was measured with a Micromeritics ASAP 2020 Analyzer at 0 °C and 1.2 bar, after which the measurement materials were degassed at 150 °C for 5 hours.

RESULTS AND DISCUSSION

The surface morphologies of the blank and Cu-based KIT-6 adsorbents were investigated with scanning electron microscopy (Figure 1). SEM-EDX analysis was also studied to determine the chemical composition of Cu/KIT-6 (Figure 2). SEM mapping analyses of the adsorbents are shown in Figure 3.

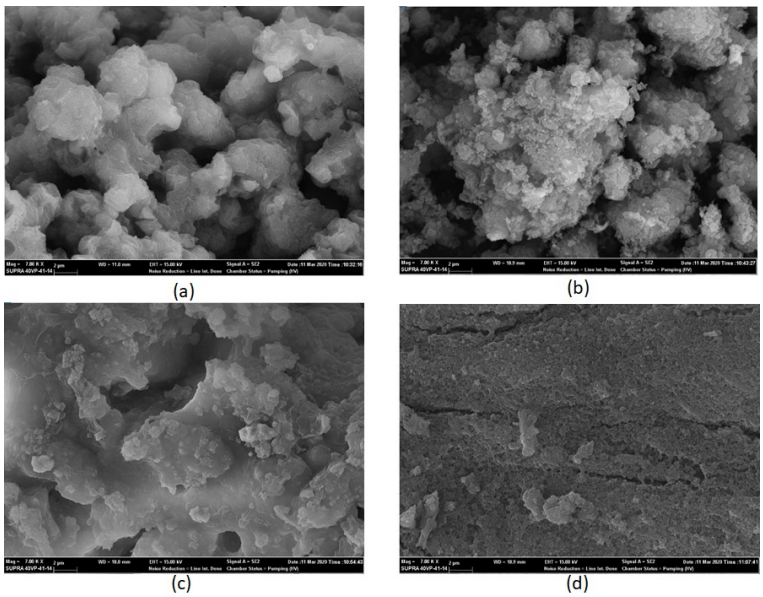

Figure 1: SEM images of (a) blank (b) 1 (c) 3 (d) 5 Si/Cu KIT-6 materials (15 kV, 7 KX).

The morphology of KIT-6 shows angular particles with a relatively flat surface (25). The sponge-like porous nature of KIT-6 was transformed to a rougher surface with the loading of Cu to silica KIT-6 support. The rock-like morphology is visible and Cu on the surface affects the surface smoothness of the materials.

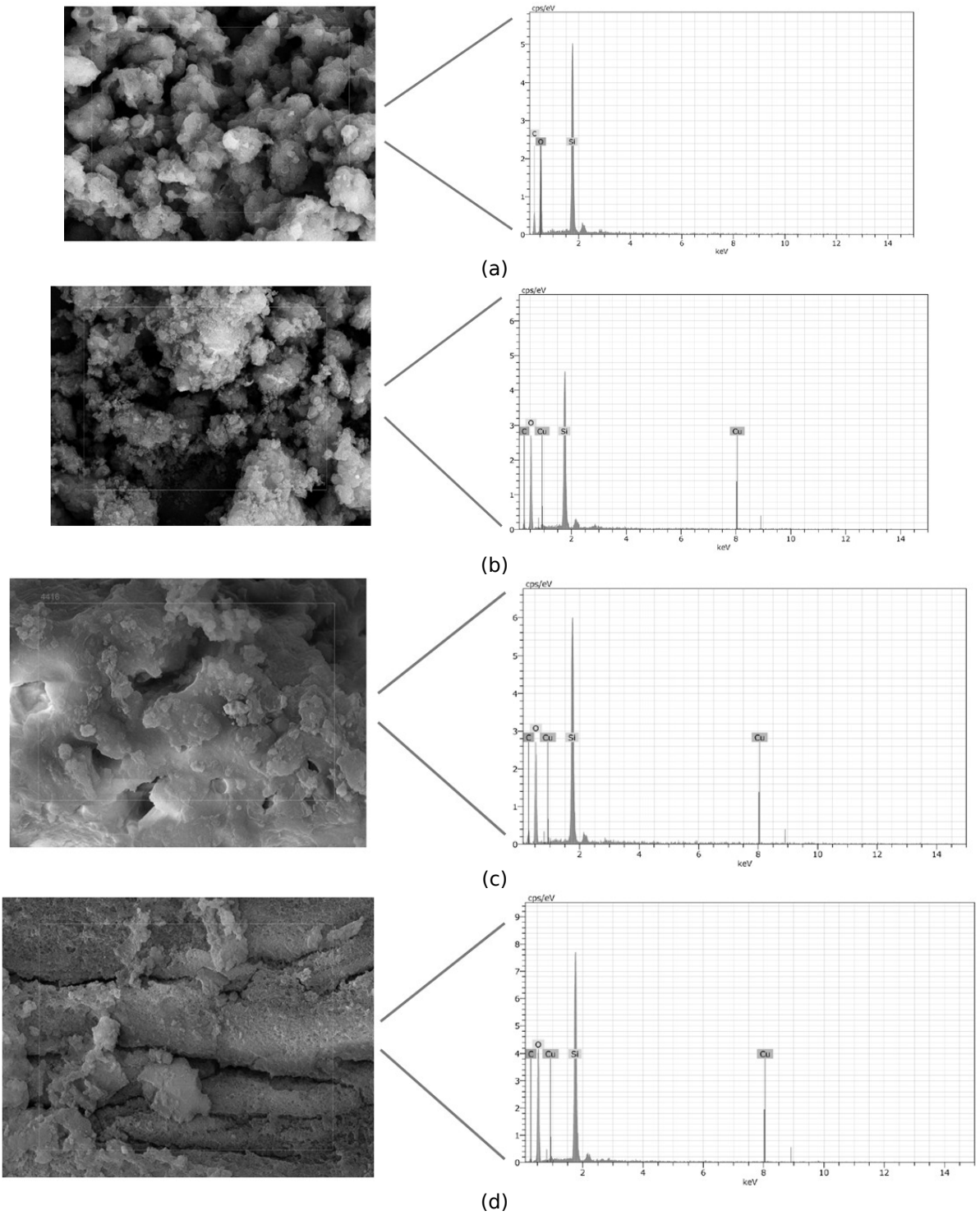

Figure 2: EDX spectra of (a) blank, (b) 1 Si/Cu, (c) 3 Si/Cu, (d) 5 Si/Cu KIT-6 materials.

The EDX analysis of Si/Cu:1, 3, 5 KIT-6 demonstrated the presence of 2.53 wt%, 1.32 wt%, and 0.34 wt% Cu, respectively in the KIT-6 framework, indicating copper was successfully incorporated into the KIT-6. EDX analysis confirms the successful synthesis of a decrease in Cu content for the Si/Cu:1, 3, 5 KIT-6, respectively because of the increase of Si content on the support KIT-6. The elemental distribution of Cu is shown in Figure 3 using SEM mapping. They were

homogeneously dispersed on the adsorbents' surface.

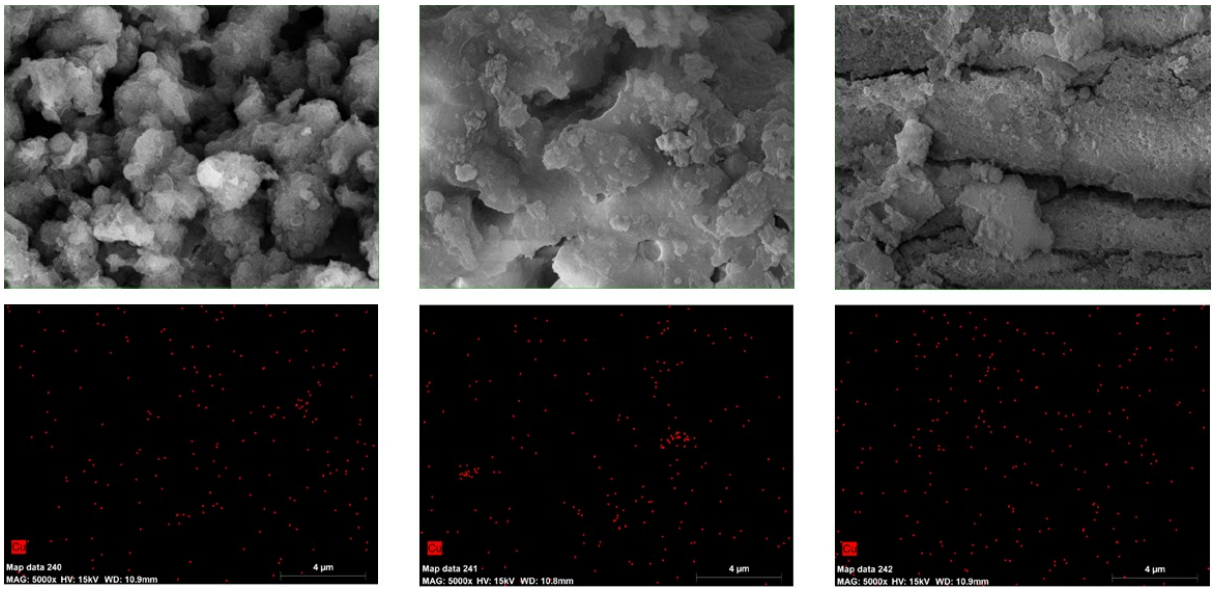

Figure 3: SEM mapping of 1 Si/Cu (left), 3 Si/Cu (middle), 5 Si/Cu (right) KIT-6 materials.

The in-site morphologies of KIT-6 materials were also investigated by TEM analysis. TEM was used to observe the internal mesoporous structure as shown in Figure 4.

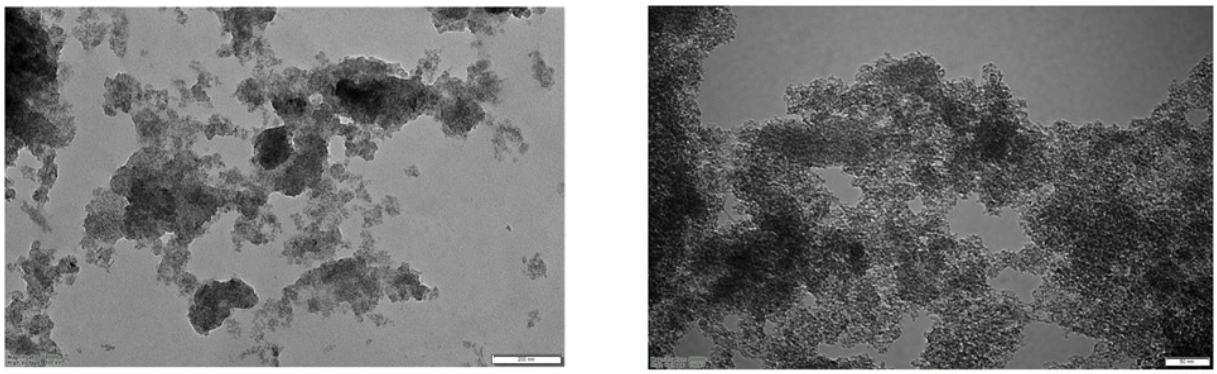

Figure 4:TEM images of (a) 5 (100 kV, 80000 X) and (b) 1 Si/Cu KIT-6 (100 kV, 200000 X) materials.

The textural properties of different Cu-based and blank KIT-6 materials, such as specific surface area (S_{BET}), pore volume (V_{total}), and pore diameter, are summarized in Table 1. The mesoporous nature of KIT-6 materials was investigated using N_2 sorption analysis. The N_2 sorption isotherms for the adsorbents are shown in Figure 5. The blank KIT-6 support exhibits the characteristic type IV isotherm via the IUPAC classification with an average pore size of 4.5 nm. The isotherms of the Cu-based KIT-6 adsorbents exhibit either type II-IV with average pore sizes between 4.7-5.5 nm with hysteresis to higher relative pressure (26). N_2 adsorption-desorption isotherms of materials indicated the formation of mesoporous structure with narrow pore size distribution. The observation implies that Si/Cu:5 KIT-6 has large pores than Si/Cu:1 and Si/Cu:3 KIT-6 adsorbents (Table 1). Si/Cu:5 KIT-6 has the lowest surface area, the increase in surface area with increasing Cu loading on the support due to the porous nature of copper. The increase of porosity from copper was due to an increase in surface area and pore volume.

Table 1: Textural properties of KIT-6 materials.

Materials	BET surface area (m^2/g)	Pore volume (cm^3/g)	Pore size (nm)
KIT-6	738.72	0.618	4.5
Si/Cu:5 KIT-6	742.88	0.734	5.5
Si/Cu:3 KIT-6	763.77	0.838	4.9
Si/Cu:1 KIT-6	780.37	1.007	4.7

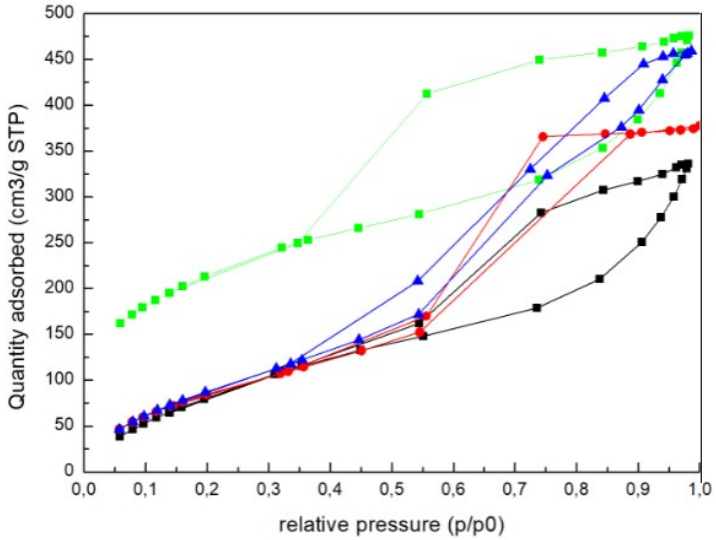

Figure 5: N_2 ads.-des. isotherms of materials (green: KIT-6, black: Si/Cu: 5 KIT-6, red: Si/Cu:3 KIT-6, blue:Si/Cu:1 KIT-6).

The crystalline phases of KIT-6 adsorbents are characterized by powder wide-angle XRD and the results are presented in Figure 6. The peaks observed at 2Θ values of 43.3, 50.4, 74, 89.8 corresponded to cubic Cu metal; 36.8, 42.8, 53.1, 66, 74.5 corresponded to cubic Cu_2O, and 32.7, 35.6, 38, 51.6, 68, 72.2 corresponded to CuO. The broad peak obtained at 23.5° corresponds to amorphous silica. The intensity of Si/Cu:1 KIT-6 was higher than the other KIT-6 materials. As the amount of Cu loaded on the structure increased, the intensity of the peaks increased as well.

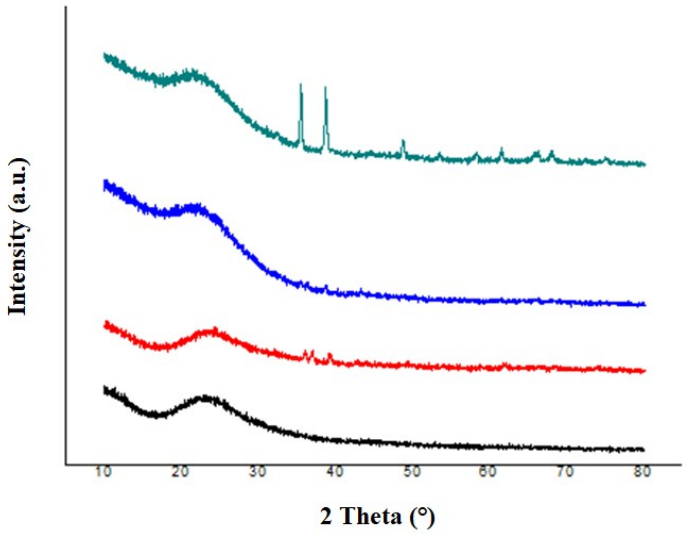

Figure 6: XRD patterns of materials (black: KIT-6, red: Si/Cu:5 KIT-6, blue: Si/Cu:3 KIT-6, green: Si/Cu:1 KIT-6).

The structural properties of KIT-6 materials were measured between 4000-400 cm^{-1} with FT-IR (Figure 7). The characteristic peak of the Si-O-Si bond appeared at about 1074 cm^{-1} for all samples due to

symmetrical stretching vibrations. The peaks at 455 cm^{-1} and 806 cm^{-1} correspond to the bending of the Si-O bond and the asymmetrical bending of the Si-O-Si bond, respectively. Symmetric stretching of Si-OH was observed around 952 cm^{-1}. Besides the band at about 3392 cm^{-1}, the peaks around 1645-1650 cm^{-1} show –OH stretching vibrations related to adsorbed water molecules that readily allow surface modification (25, 31).

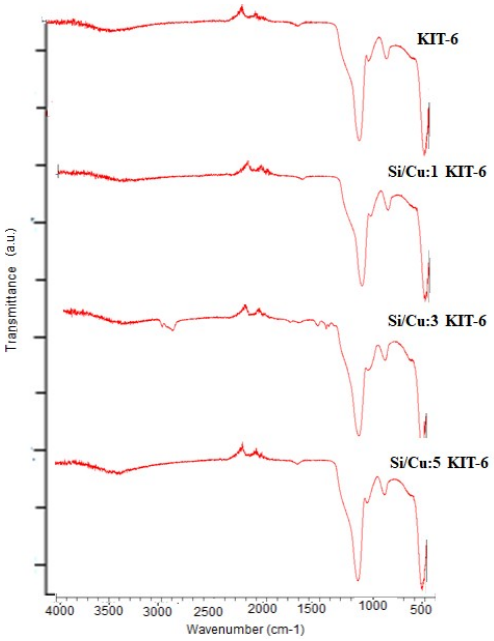

Figure 7: FT-IR spectra of KIT-6 materials.

All samples were used as adsorbents for CO_2 adsorption at 273 K and pressure up to 1.2 bar. The CO_2 adsorption capacities for the materials are shown in Figure 8. It is preferred at a lower temperature due to the CO_2 exothermic process. Among the four samples, Si/Cu:1 KIT-6 recorded the highest CO_2 adsorption with 1.70 mmol/g at 0 °C and 1.2 bar. Si/Cu:1 has the highest adsorption capacity of KIT-6 due to the Cu particles inside the porous channels and this provides adsorption sites for CO_2 molecules. As seen from the results, the amount of Cu in the KIT-6 support is the critical point for CO_2 adsorption, and the material with highest surface area is the best adsorbent. The CO_2 adsorption capacity shows a similar trend with Si/Cu:1 KIT-6 compared to other KIT-6 adsorbents (Table 2). The importance of KIT-6 mesoporosity also supports the high adsorption of CO_2 molecules. A comparison of the CO_2 capture capacities of adsorbents similar to this study is shown in Table 3. The surface area and CO_2 adsorption capacities of KIT-6 are quite high under similar pressure and temperature conditions.

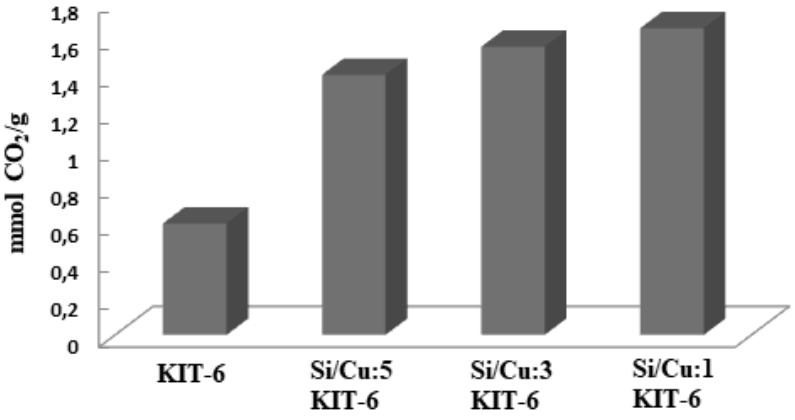

Figure 8: CO_2 capture of KIT-6 silicas (1.2 bar and 0 °C with dry CO_2 gas).

Table 2: CO_2 capture capacity of KIT-6 silicas.

Sample	CO_2 adsorbed (mmol/g)
KIT-6	0.60
Si/Cu:5 KIT-6	1.40
Si/Cu:3 KIT-6	1.55
Si/Cu:1 KIT-6	1.70

From the table of comparison of the different materials (Table 3), low temperature and pressure with a high surface area favor higher CO_2 adsorption capacity. A certain amount of added copper plays a critical role in controlling the total adsorption capacity of the KIT-6 support. It has been determined that adding a small amount of Cu to the KIT-6 structure shows a good effect on CO_2 adsorption. All literature studies also show the importance of the main properties and parameters that can be used for the CO_2 capacities of materials.

Table 3: Comparison of the different materials for CO_2 capture capacities.

Material	Temp. (°C)	Pressure (bar)	Surface area (m^2/g)	CO_2capture (mmol/g)	Ref.
An-KIT-6	30	1.00	297	0.90	(15)
Amine-MCM-41	0	1.20	279	0.83	(27)
HMS-F MS	25	1.00	636	1.00	(28)
CS-1.5	0	0.15	1187	1.25	(29)
Amine-MCM-41	30	1.20	1759	1.15	(30)
Amine-SBA-15	25	1.00	1177	1.20	(31)
Amine-KIT-6	0	1.20	1070	0.60	(32)
Cu/Si:1 KIT-6	0	1.20	780	1.70	This work
Cu/Si:5 KIT-6	0	1.20	742	1.40	This work

CONCLUSION

In this study, different amounts of Cu-loaded KIT-6 were prepared and investigated for high CO_2 capture capacity at 0 °C and 1.2 bar. The highest CO_2 adsorbed of 1.70 mmol/g was achieved at Si/Cu:1 KIT-6. It was seen that the materials with optimized Cu content on KIT-6 support showed excellent textural properties and high CO_2 adsorption capacity for the determined temperature and pressure. The adsorption capacities at 0 °C provide strong evidence at low temperature and pressure and due to the mesoporous nature of the materials, CO_2 was used as a probe molecule for investigating the porosity. The Cu-based KIT-6 combination could be used as an effective material for CO_2 capture.

REFERENCES

1. Zhou K, Chaemchuen S, Verpoort F. Alternative materials in technologies for Biogas upgrading via CO2 capture. Renewable and Sustainable Energy Reviews. 2017 Nov;79:1414–41. <DOI>.

2. Lakhi KS, Cha WS, Joseph S, Wood BJ, Aldeyab SS, Lawrence G, et al. Cage type mesoporous carbon nitride with large mesopores for CO2 capture. Catalysis Today. 2015 Apr;243:209–17. <DOI>.

3. Mutyala S, Jonnalagadda M, Mitta H, Gundeboyina R. CO2 capture and adsorption kinetic study of amine-modified MIL-101 (Cr). Chemical Engineering Research and Design. 2019 Mar;143:241–8. <DOI>.

4. Han Y, Hwang G, Kim H, Haznedaroglu BZ, Lee B. Amine-impregnated millimeter-sized spherical silica foams with hierarchical mesoporous–macroporous structure for CO2 capture. Chemical Engineering Journal. 2015 Jan;259:653–62. <DOI>.

5. Yıldız MG, Davran-Candan T, Günay ME, Yıldırım R. CO2 capture over amine-functionalized MCM-41 and SBA-15: Exploratory analysis and decision tree classification of past data. Journal of CO2 Utilization. 2019 May;31:27–42. <DOI>.

6. Gaikwad S, Kim SJ, Han S. CO2 capture using amine-functionalized bimetallic MIL-101 MOFs and their stability on exposure to humid air and acid gases. Microporous and Mesoporous Materials. 2019 Mar;277:253–60. <DOI>.

7. Zhang G, Zhao P, Xu Y. Development of amine-functionalized hierarchically porous silica for CO2 capture. Journal of Industrial and Engineering Chemistry. 2017 Oct;54:59–68. <DOI>.

8. Liu Y, Shi J, Chen J, Ye Q, Pan H, Shao Z, et al. Dynamic performance of CO2 adsorption with tetraethylenepentamine-loaded KIT-6. Microporous and Mesoporous Materials. 2010 Oct;134(1–3):16–21. <DOI>.

9. Peirce S, Russo ME, Perfetto R, Capasso C, Rossi M, Fernandez-Lafuente R, et al. Kinetic characterization of carbonic anhydrase immobilized on magnetic nanoparticles as biocatalyst for CO2 capture. Biochemical Engineering Journal. 2018 Oct;138:1–11. <DOI>.

10. Hussain M, Akhter P, Saracco G, Russo N. Nanostructured TiO2/KIT-6 catalysts for improved photocatalytic reduction of CO2 to tunable energy products. Applied Catalysis B: Environmental. 2015 Jul;170–171:53–65. <DOI>.

11. Hu L, Liu J, Zhu L, Hou X, Huang L, Lin H, et al. Highly permeable mixed matrix materials comprising ZIF-8 nanoparticles in rubbery amorphous poly(ethylene oxide) for CO2 capture. Separation and Purification Technology. 2018 Oct;205:58–65. <DOI>.

12. Wang X, Zhou J, Xing W, Liu B, Zhang J, Lin H, et al. Resorcinol–formaldehyde resin-based porous carbon spheres with high CO2 capture capacities. Journal of Energy Chemistry. 2017 Sep;26(5):1007–13. <DOI>.

13. Sari Yilmaz M. Synthesis of novel amine modified hollow mesoporous silica@Mg-Al layered double hydroxide composite and its application in CO2 adsorption. Microporous and Mesoporous Materials. 2017 Jun;245:109–17. <DOI>.

14. Sun H, Parlett CMA, Isaacs MA, Liu X, Adwek G, Wang J, et al. Development of Ca/KIT-6 adsorbents for high temperature CO2 capture. Fuel. 2019 Jan;235:1070–6. <DOI>.

15. Kishor R, Ghoshal AK. APTES grafted ordered mesoporous silica KIT-6 for CO2 adsorption. Chemical Engineering Journal. 2015 Feb;262:882–90. <DOI>.

16. Huang X, Ding J, Zhong Q. Catalytic decomposition of H2O2 over Fe-based catalysts for simultaneous removal of NOX and SO2. Applied Surface Science. 2015 Jan;326:66–72. <DOI>.

17. Gargiulo N, Pepe F, Caputo D. CO₂ Adsorption by Functionalized Nanoporous Materials: A Review. j nanosci nanotech. 2014 Feb 1;14(2):1811–22. <DOI>.

18. Yan B, Yu S, Zeng C, Yu L, Wang C, Zhang L. Binderless zeolite NaX microspheres with enhanced CO2 adsorption selectivity. Microporous and Mesoporous Materials. 2019 Apr;278:267–74. <DOI>.

19. Huang J, Zou J, Ho WSW. Carbon Dioxide Capture Using a CO_2 -Selective Facilitated Transport Membrane. Ind Eng Chem Res. 2008 Feb 1;47(4):1261–7. <DOI>.

20. Heyl D, Rodemerck U, Bentrup U. Mechanistic Study of Low-Temperature CO_2 Hydrogenation over Modified Rh/Al_2O_3 Catalysts. ACS Catal. 2016 Sep 2;6(9):6275–84. <DOI>.

21. Liu J, An T, Li G, Bao N, Sheng G, Fu J. Preparation and characterization of highly active mesoporous TiO2 photocatalysts by hydrothermal synthesis under weak acid conditions. Microporous and Mesoporous Materials. 2009 Aug;124(1–3):197–203. <DOI>.

22. Hiyoshi N, Yogo K, Yashima T. Adsorption characteristics of carbon dioxide on organically functionalized SBA-15. Microporous and Mesoporous Materials. 2005 Sep;84(1–3):357–65. <DOI>.

23. Zhou Y, Lu J, Zhou Y, Liu Y. Recent advances for dyes removal using novel adsorbents: A review. Environmental Pollution. 2019 Sep;252:352–65. <DOI>.

24. Lv Y, Xin Z, Meng X, Tao M, Bian Z, Gu J, et al. Essential role of organic additives in preparation of efficient Ni/KIT-6 catalysts for CO methanation. Applied Catalysis A: General. 2018 May;558:99–108. <DOI>.

25. Wei Y, Cai W, Deng S, Li Z, Yu H, Zhang S, et al. Efficient syngas production via dry reforming of renewable ethanol over Ni/KIT-6 nanocatalysts. Renewable Energy. 2020 Jan;145:1507–16. <DOI>.

26. Ouyang H, Guo L, Li C, Chen X, Jiang B. Fabrication and adsorption performance for CO2 capture of advanced nanoporous microspheres enriched with amino acids. Journal of Colloid and Interface Science. 2018 Dec;532:433–40. <DOI>.

27. Loganathan S, Ghoshal AK. Amine tethered pore-expanded MCM-41: A promising adsorbent for CO 2 capture. Chemical Engineering Journal. 2017 Jan;308:827–39. <DOI>.

28. Cecilia JA, Vilarrasa-García E, García-Sancho C, Saboya RMA, Azevedo DCS, Cavalcante CL, et al. Functionalization of hollow silica microspheres by impregnation or grafted of amine groups for the CO 2 capture. International Journal of Greenhouse Gas Control. 2016 Sep;52:344–56. <DOI>.

29. Wang W, Qi R, Shan W, Wang X, Jia Q, Zhao J, et al. Synthesis of KIT-6 type mesoporous silicas with tunable pore sizes, wall thickness and particle sizes via the partitioned cooperative self-assembly process. Microporous and Mesoporous Materials. 2014 Aug;194:167–73. <DOI>.

30. Mello MR, Phanon D, Silveira GQ, Llewellyn PL, Ronconi CM. Amine-modified MCM-41 mesoporous silica for carbon dioxide capture. Microporous and Mesoporous Materials. 2011 Aug;143(1):174–9. <DOI>.

31. Wang L, Ma L, Wang A, Liu Q, Zhang T. CO2 Adsorption on SBA-15 Modified by Aminosilane. Chinese Journal of Catalysis. 2007 Sep;28(9):805–10. <DOI>.

32. Hu Y, Liu W, Sun J, Yang X, Zhou Z, Zhang Y, et al. High Temperature CO_2 Capture on Novel Yb_2O_3 -Supported CaO-Based Sorbents. Energy Fuels. 2016 Aug 18;30(8):6606–13. <DOI>.

33. Chi C, Li Y, Ma X, Duan L. CO2 capture performance of CaO modified with by-product of biodiesel at calcium looping conditions. Chemical Engineering Journal. 2017 Oct;326:378–88. <DOI>.

JOTCS B
Journal of the Turkish Chemical Society
Section: B
Chemical Engineering
TURKISH CHEMICAL SOCIETY

The Effect of Temperature on the Enantioselectivity of Lipase-Catalyzed Reactions; Case Study: Isopropylidene Glycerol Reaction

Adnan Aydemir*[1,2]

[1]Institut für Technische Chemie, Universität Hannover, 30167, Hannover, Deutschland
[2]Nisantasi University, Istanbul, Turkey

Abstract: Commercial lipase (triacylglycerol lipase (EC 3.1.1.3) of *Burkholderia cepacia* (40 U/mg) in its crude form has been used in the kinetic resolution of enzyme-catalyzed reaction of 1,2-*O*-isopropylidene-sn-glycerol and vinyl acetate as acyl donor in the organic solvent *n*-hexane. It was observed that the enantioselectivity is in the range of 2.295 to 2.235 while $\Delta\Delta G_{D,L}$ -73.408 to -75.682 kJ/mol at 35 °C and 55 °C, respectively . This shows that any increase in the reaction temperature led to an increased final conversion, but it has no effect on the enantioselectivity of the reaction. Also, the thermodynamic effect of temperature on the Gibbs free energy in the lipase-catalyzed kinetic resolution of the reaction between racemic isopropylidene glycerol and vinyl acetate remains in the small range. By using this type of analysis, the researchers may predict if they should increase or decrease the temperature to enhance the selectivity of enzyme in catalyzing a reaction.

Keywords: Enantioselectivity, lipase, temperature, isopropylidenglycerin , kinetic resolution, *Burkholderia cepacia.*

Submitted: April 05, 2022. **Accepted:** May 31, 2022.

Cite this: Aydemir A. The Effect of Temperature on the Enantioselectivity of Lipase-Catalyzed Reactions; Case Study: Isopropylidene Glycerol Reaction. JOTCSB. 2022;5(1):29–38.

***Corresponding author. E-mails:** Aydemir@iftc.uni-hannover.de, adnanaydemir@gmail.com

INTRODUCTION

One of the elusive hallmarks in formation of life within the prebiotic era on the Earth is how Nature chose a specific chirality (or handedness) or called biological homochirality. Thereof the homochirality of amino acids (L-enantiomers), sugars (D-enantiomers), proteins, and DNA became one of the biochemical characteristic properties in the life on Earth (1,2). Although Nature prefers almost exclusively stereochemical imperative chiral molecules in living organisms as single enantiomers, yet the left- and right-handed molecules of a compound will deterministically form in equimolar composition (a racemic mixture) when they are synthesized in the laboratory in the absence of some type of directing template (3,4).

However, about a century later it is drastically determined that the phenomenon of chirality implements a key role in pharmaceutical, agricultural, food, and other chemical industries as well as in the life of plants and animals (5–7). Since it is evident that the chirality is a fundamental characteristic of life processes, the individual enantiomers of chiral chemicals in a racemic mixture may divulge very different bioactivities and/or biotoxicities (8). It means that one enantiomer may be active (eutomer) while the other one (distomer) might be inactive, useless, harmful, or toxic (poisonous), sometimes in certain cases producing undesired side effects (9–11).

Over the last two decades, stereochemistry has been gaining prime importance in chemical technologies associated with the synthesis, separation, identification, and analysis of target eutomers from undesired distomers in a racemic compound, (12), particularly in the fields of contemporary pharmaceutical, agrochemical, food, smell, material sciences, and many other rapidly expanding areas of research (13–15).

Accordingly, it became necessary to search an appropriate process to separate racemic compounds into their enantiomers to produce optically active compounds. Therefore, the different methods to differentiate between various enantiomers can be used like crystallization (14,16,17), separation with membranes (18–21), liquid-liquid extraction (22), capillary electrophoresis (23,24), chromatography (25), and kinetic resolution (KR)(26–33). Among these methods, the resolutions based on kinetic effects in chemical reactions can be one of several major types but are typically divided between enzyme and inorganic catalyzed systems. The enzyme-catalyzed transformations to produce enantiomerically pure compounds have been progressively considered in the

manufacture of a wide range of single enantiomers in the industry. Kinetic resolution is defined as a process where the two enantiomers of a racemate are transferred to the product much faster than the other (34). Due to the structural diversity of chiral compounds, in the frame of substrate specificity, a huge amount of enzymes were recently used for enantioseparation to determine their activity and selectivity in the kinetic (35).

Among these numerous amounts of enzymes, the kinetic resolution using lipases provide high enantiomeric excess (ee) and can be cost effective compared to other techniques. However, there are some factors that affect activity and selectivity of lipase-catalyzed reactions, including the nature of the acylating agent, temperature, pH and solvent selection (26). This paper scrutinizes if there is any temperature effect on the kinetic resolution of lipases in the transesterification of isopropylideneglycerin with vinyl acetate as acyl donor.

Lipases (triacylglycerol ester hydrolases, EC 3.1.1.3) are a versatile group of biocatalysts, which are ubiquitous enzymes catalyzing the hydrolysis of fats and oils (36). The number of available lipases has increased considerably since the 1980s. Their natural physiologic function is to hydrolyze triglycerides into diglycerides, monoglycerides, fatty acids, and glycerol during digestion (37,38). Lipases are frequently used in lipid modification and in organic synthesis. Enzymes in this class have been shown to be 1,3- regioselective for triglycerides, selective for fatty acid chain length and degree of fatty acid saturation (36,39).

In addition to their natural function of hydrolyzing carboxylic ester bonds, lipases can catalyze esterification, inter-esterification, and transesterification reactions in non-aqueous media. The broad substrate specificity makes lipases usable in a wide range of applications, and thus their market is still growing (40). This versatility makes lipases the enzymes of choice for potential applications in the dairy and food industries, in the production flavor and aroma components, in oleo-chemical industry, in medical applications (37,41–43), in the detergent, leather, textile, cosmetic, and paper industries (38,44), and in the production of optically active compounds for the agrochemical and pharmaceutical industries (38,45,46). Beyond all these applications, they are widely used in the synthesis of organic compounds (47) to produce homochiral compounds from racemates via enantiomeric discrimination or from prochiral or meso compounds via enantiotropic differentiation. The resolution of racemic compounds *via* hydrolysis in aqueous media or trans/esterification in organic media cannot always be achieved in a highly enantioselective manner (48,49). Enantioselectivity can be improved by several methods, *e.g.*, the screening of enzymes (50,51), the modification of substrates (17,18), or the modulation of reaction conditions.

Temperature, which is an easily controllable parameter in the experimental conditions, is a potential factor that may affect the enantioselectivity of the enzymatic reactions (49,52). However, its effect on the stereoselectivity of enzymatic transformations has not been investigated sufficiently (48,53–55). There have been remarkably few systematic studies on the effects of temperature variation on the stereochemistry of enzymatic reactions (56). Some examples of an improvement of enantioselectivity by temperature-dependent reversal of stereochemistry were observed (57–59).

Eyring's transition state theory (60) defines the relation of temperature with the reaction rate constant as:

$$k = \kappa \frac{k_B T}{h} K \qquad \text{(Eq. 1)}$$

where k= reaction rate constant, κ= transmission coefficient, k_b= Boltzmann constant, T= temperature, K= equilibrium constant.

The equilibrium constant is related with Gibbs free energy through Van't Hoff equation.

$$\Delta G = -RTlnK \qquad \text{(Eq. 2)}$$

Enzymatic enantioselectivity E is defined as the ratio of specificity constants of the two competing enantiomers (61). Aydemir modified this concept showing that the enantioselectivity is especially the ratio of kinetic constants of reactions for the competing racemates at the activated enzyme site (62). The specificity constant of an enzyme for its substrates is defined as the ratio k_{cat}/K for the D and L racemates (59,63).

$$E = \frac{D}{L} = \left(k_{cat}/K\right)_D / \left(k_{cat}/K\right)_L \qquad \text{(Eq. 3)}$$

The kinetic constant, k_{cat}/K, is related to the thermodynamic term ΔG, as shown in following equation from transition-state theory (64).

$$\Delta\Delta G = -RTlnE \qquad \text{(Eq. 4)}$$

where $\Delta\Delta G^*$ is the difference in free energy of activation between the D and L racemates (59).

The temperature dependence of the activation free energy is given by Gibbs-Helmholtz equation:

$$\Delta\Delta G^* = \Delta\Delta H^* - T\Delta\Delta S^* \qquad \text{(Eq. 5)}$$

Substituting Eq. (4) into Eq. (5), the relationship between enantioselectivity, enthalpy, and entropy is derived (56):

$$lnE = \left(\frac{\Delta\Delta S^*}{R}\right) - \left(\frac{\Delta\Delta H^*}{RT}\right) \qquad \text{(Eq. 6)}$$

if no enantiomeric discrimination of the enzyme between the D and L isomers occurs, then E = 1 and $\Delta\Delta G^* = 0$. In this case, the enthalpy and entropy contributions are equal to

$$T_r = \Delta\Delta H^*/\Delta S^* \qquad \text{(Eq. 7)}$$

The temperature is thus the "racemic temperature" (56,65). This analysis predicts that temperature dependent inversion of stereochemical configuration occurs. At temperatures below T_r., the $\Delta\Delta G^*$ is dominated by $\Delta\Delta H^*$, and the E value

of product will decrease as T increases, until it reaches unity at T_r. In contrast, at temperatures above T_r. the $\Delta\Delta G^*$ is dominated by $T\Delta\Delta S^*$, and the E value increases as T increases. Therefore, the optimization of enantiomeric enzyme catalyzed reactions may require either the raising or lowering the reaction temperature (56,66).

The influence of the reaction temperature on the enantioselectivity appears to depend on the nature of the reaction involved (67). Increasing the temperature normally leads to an increase of the enzymatic reaction rate, and obviously resulted in a higher reaction rate and a higher final conversion (57). At the same time, the enantioselectivity often decreases and a loss of enzyme stability can be observed (68).

Identification of $\Delta\Delta G_{D,L}$ as the free energy difference that determines the enantiomeric ratio opens the possibility to predict E (69). Studies on the temperature dependence of E allow for a thermodynamic analysis for the enantioselectivity of enzymes, which is caused by enthalpic and entropic activation energy differences of the enantiomers. These studies have also revealed the entropic contributions to be nearly as big as the enthalpic contribution, whereas the entropic activation energy depends on the interactions with solvent molecules and enantiomers in transition state at the active site (63,70). Although this is a dichotomy between enthalpy and entropy which results in the observed temperature dependence (65), the enthalpic and the entropic components of the differential activation free energy, $\Delta\Delta G_{D,L}$ were both important to the overall success of the kinetic resolution of the enantiomers (70).

Although increasing the temperature usually decreased the enantioselectivity, high enantioselectivity can be expected even at high temperatures if the structure of the substrate is ideal from the mechanistic point of view (71). The acyl donor may greatly influence the enantioselectivity and reaction rate of acylation (72). A slight elongation of the alkyl chain of the vinyl esters caused dramatic changes in the enantioselectivity (73). It was the highest when vinyl acetate was used as acyl donor and became lower with the chain length of the fatty acid moiety (52). The position of the double bond has also affected the reaction rate and enantioselectivity (42). The bulky aromatic group allowed only one enantiomer to fit in the active site, whereas for aliphatic compounds the enzyme could not distinguish well between both forms (43). An addition of a suitable amount of water can alter dramatically the behavior of their enantioselectivities as a function of the temperature (55).

As well as the effect of the structure of substrate by the medium engineering point of view, the temperature effect on the enantioselectivity discriminates itself quite differently depending on the type of reaction. As given on the (Table 2), it is reported that E value may increase or decrease or is unaffected with lowering or increasing the reaction temperature.

The non-covalent interactions of the substrate with the residues at the active site determine the thermodynamic and kinetic properties of the complex (74). Above-mentioned Equation 4 gives the relationship between enantioselectivity and temperature via the free activation energy $\Delta\Delta G$. The equations 5 and 6 relate further the free energy to enthalpic and entropy contributions. Ottosson (70) has studied that the enthalpic and the entropic components of the differential activation free energy, $\Delta\Delta G_{D,L}$ are both important to the overall success of the kinetic resolution of the enantiomers. The knowledge of how this enzyme distinguishes between enantiomers and the roles of enthalpy and entropy on a molecular level (75).

Table 1: some research for the change of E with variation in temperature.

Temperature	Enantioselectivity	Ref.
high	high	(76,77)
high	low	(58,71,78–81)
low	High	(82,83)
low	low	(84)
high or low	no change	(67,85,86)

If the $T\Delta\Delta S$ and $\Delta\Delta H$ terms for a desired reaction forming enantiomeric products are closely balanced, then the reaction will be subject to stereochemical modulation by changes in temperature. If the $\Delta\Delta G$ is dominated by the $T\Delta\Delta S$ term, then reactions will show the maximal stereochemical discrimination at the highest temperature compatible with the stability of the enzyme – cofactor – substrate system. If the substituent has polar groups that interact with the enzyme by ionic attraction or by hydrogen bonding, the $\Delta\Delta H$ term will be quite large and will dominate the free energy of activation, resulting in little or no effect of temperature. If the major contributor to $\Delta\Delta G$ is $\Delta\Delta H$, then the stereochemical purity of the reaction product will be maximal at the lowest temperature at which the enzyme exhibits useful reactivity (56).

In this work, the effect of temperature on the reaction conditions on the transesterification of isopropylideneglycerin (IPG), catalyzed by *Burkholderia cepacia* lipase (BCL), previously known as *Pseudomonas cepacia*, has been investigated. IPG, [+]-Solketal (1,2-O-isopropylidene-sn-glycerol (IPG); [+]-2,2-dimethyl-1,3-dioxolane-4-methanol) (Figure 1), is an important starting compound for the preparation of many C_3-synthons which are widely applied in organic synthesis (87), as an interesting chiral intermediate for pharmaceutical industries, since it is an important starting chiral synthon in the synthesis of diglycerides, glyceryl phosphates, tetraoxaspiroundecanes, and of many biologically active compounds, such as phospholipids, β-adrenoceptor antagonists propranolol, and platelet aggregating factors (88–91). The esterification of isopropylidene-glycerin (IPG)

with vinyl acetate as an acyl donor (92–94) in *n*-hexane (95–97) has been examined, and the effect of temperature on the enantioselectivity of *B.Cepacia* lipase for D, L-IPG was investigated.

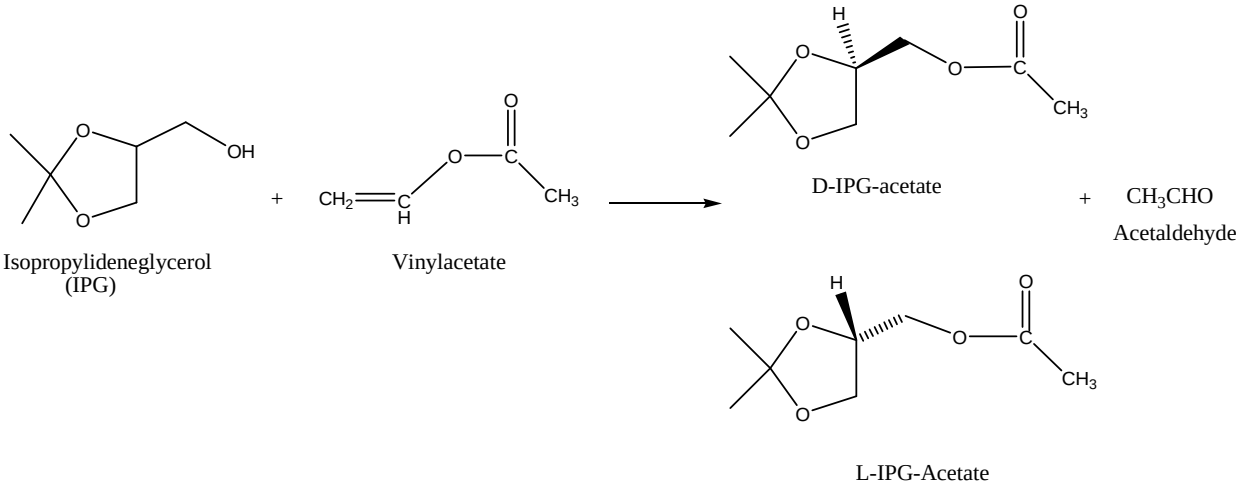

Figure 1: Reaction of Isopropylidenglycerin with vinyl acetate.

MATERIALS AND METHODS

Chemicals and Lipase

Lipase from *Burkholderia cepacia* (40 U/mg, Fluka) was used in its crude form. The organic solvent *n*-hexane (Fluka), 1,2-*O*-isopropylidene-sn-glycerol (Fluka), vinyl acetate as acyl donor (Merck) were used without any further purification.

The analysis has been performed by gas chromatography (CC-14A, Shimadzu) with a chiral column of FS-Hydrodex® ß-3P, (Heptakis (2,6-di-*O*-methyl-3-*O*-pentyl)-ß-cyclodextrin) with a length of 25 m and an inside diameter of 0.25 mm (Macherey-Nagel, Düren, Germany).

Reactions in organic solvents

Preliminary experiments of related reactions in organic solvent were carried out in a 20 mL volume of a glass vessel sealed with a rubber stopper. In the experiments, 10 mmol of racemate (IPG) and 30 mmol of excess component vinyl acetate as an acylating agent were mixed to complete the total reaction medium of 10 mL with *n*-hexane. By adding 50 mg of *Burkholderia cepacia* lipase, the reaction started. The reaction mixture is incubated in water bath and agitated with magnetic stirring. The magnetic stirrer speed was 600 rpm. Samples withdrawn during the reaction were centrifugated and diluted with acetone before gas chromatographic (GC) analysis.

Determination of enantiomeric excess and conversion

Samples from the reaction mixture were diluted with acetone. Enantiomeric purities were calculated from peak areas determined by gas chromatography using a chiral stationary phase (FS-Hydrodex® ß-3P, Macherey-Nagel, Germany). From the detected data, the conversion was calculated as described by Chen et al. (68).

RESULTS

Lipase-catalyzed trans-esterification between D, L-IPG and vinyl acetate was studied. The product IPG-acetate and acetaldehyde as a by-product were produced during this reaction. As shown in Figure 1, the overall reaction is irreversible and therefore shifts itself towards product formation (96,98). Transesterification in *n*-hexane was performed at different temperatures viz. 35 °C, 40 °C, 45 °C, 50 °C and 55 °C, respectively. The conversion and the enantioselectivity of BCL was calculated as described by Chen (99) and Aydemir's enantioselectivity definition (62).

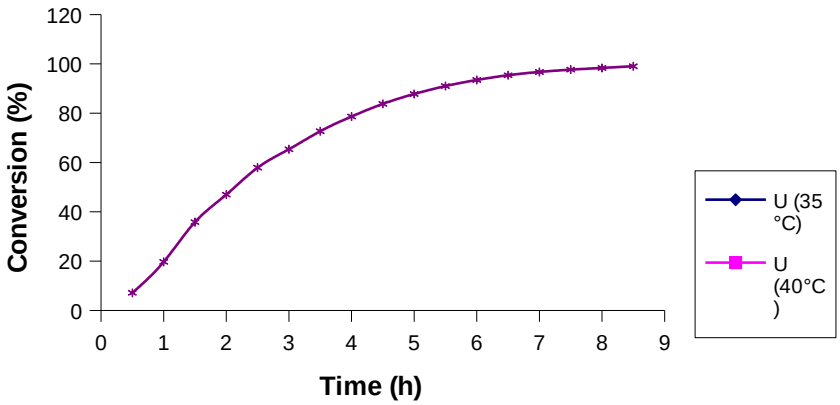

Figure 2. Conversion vs. time profile of IPG at different temperatures.
(10 mmol IPG, 30 mmol vinyl acetate, 50 mg Lipase BC. 10 mL solution)

The rate of a chemical reaction increases with rising temperature according to Van't Hoff equation. In this work, it is determined that the reaction rate and the conversion were risen at the same time with increasing temperature till 50 °C, then decreases above this temperature (Figure 2). The detected optimum temperature 50 °C is convenient with the lipase properties on the prospect of the enzyme supplying company (Fluka). Above this temperature, the activity of the lipase descends resulting in decrease of the conversion. That might possibly result in the fact that the enzyme structure starts to be destroyed along with the rising temperature above 50 °C.

Table 2: Temperature vs. E values.

Temp .(°C)	Max. conversion	E value	$\Delta\Delta G_{D,L}$ (kj)
35	61	2.295	-73.408
40	65	2.267	-73.497
45	69	2.254	-74.147
50	93	2.242	-74.818
55	79	2.235	-75.682

The enantiomeric ratio was determined according to Rakels *et.al.* with the following equation (100).

$$E = \frac{\ln\left[\frac{1-eeS}{1+\left(\frac{eeS}{eeP}\right)}\right]}{\ln\left[\frac{1+eeS}{1+\left(\frac{eeS}{eeP}\right)}\right]} \qquad \text{(Eq. 8)}$$

The results of the experiments to determine the temperature dependency of enantioselectivity in the esterification of IPG were given in Figure 3. The conversion reached from 61% at 35 °C to the maximum conversion of 93% at 50 °C, after 4 hours of reaction time. As a result, it became evident that the enantioselectivity (E) remained almost unchanged with the temperature in the mean value of 2.26, tending to convert more L-form than D- form of the IPG (Table 2).

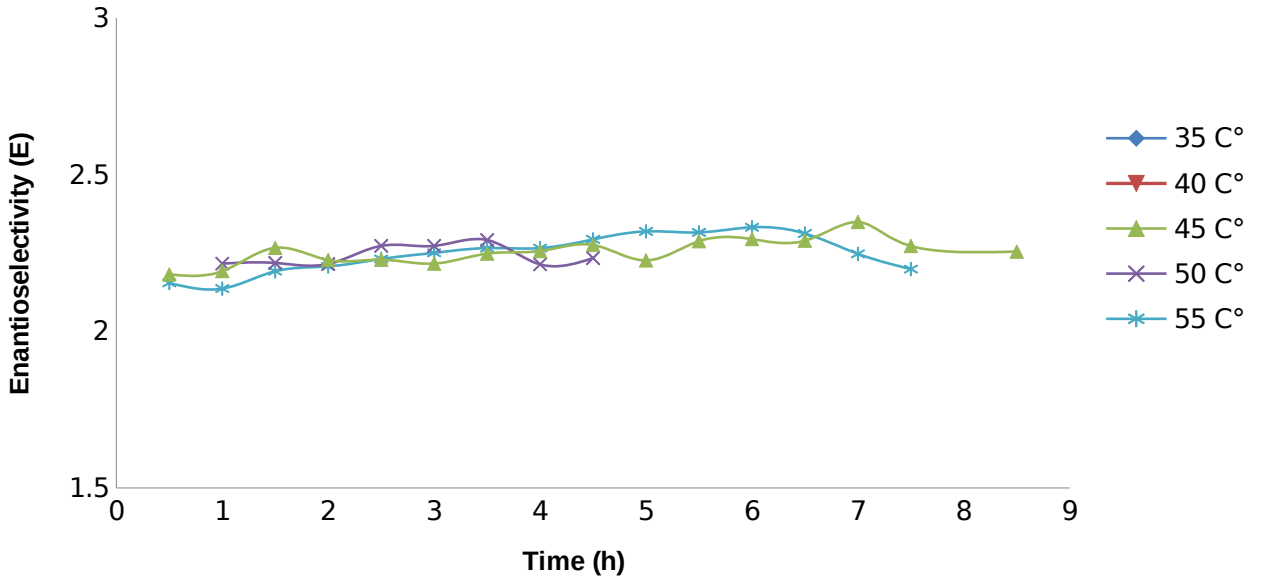

Figure 3: Enantioselectivity vs. time at different temperatures.

CONCLUSION

The enhancement of enantioselectivity to produce the desired racemic product is recently studied by many laboratories. In order to achieve the enhancement, the physical conditions of the reaction medium has been altered. The acyl donor, solvent type, the effect of water content on the enzyme flexibility, and the temperature are the commonly studied parameters. Among these parameters, it is examined that the enantioselectivity alters irregularly with temperature. Thus, it could be concluded that the molecular structure of the substrate indirectly determines the dependency of enantioselectivity on temperature, by defining the contribution of enthalpic or entropic effect of the activation energy. The enthalpic and entropic values are equal to each other at a certain temperature. Consequently, the enantiomeric ratio (E) value becomes 1. This temprature is called racemic tempreature, at which a racemate is formed. Above or below the racemic temperature, a decrease in temperature will cause either a decrease or increase in enantioselectivity. As a result it is thus suggested to consider the effects of temperature on the selectivity of enzymatic reactions (101) in the future works.

In the present work, the effect of temperature on the lipase catalyzed reaction between isopropylidene glycerol and vinyl acetate was analyzed thermodynamically, since the activation energy $\Delta G_{D,L}$ of each enantiomer is related to temperature and entropy ($T\Delta S$), the value of $\Delta G_{D,L}$ has been calculated to analyze how it changes with enantioselectivity at temperatures between 35 – 55 °C. It is observed that the enantiomeric excess value is 2.295 and $\Delta G_{D,L}$= -73.408 kJ/mol at 35 °C, while EE= 2.235 and $\Delta G_{D,L}$= -75.682 kJ/mol. It shows that the higher enantioselectivty can be obtained at low temperatures (35 °C) having low entropy value. Since there is no huge amount of difference in EE or ΔG values calculated in this work, it can be interpreted that the reaction between vinyl acetate and isopropylidene glycerol is not strongly dependent on the temperature, and increase in temperature causes decrease in ΔG, because $T\Delta S$ becomes greater than ΔH ($\Delta\Delta H^* < T\Delta\Delta S^*$). Finally, this work adds that low temperatures are suggested for the selectivity of one enatiomer to other in the reaction studied.

ACKNOWLEDGEMENT

I am gracefully thankful to Prof. Dr. Thomas Scheper supplying all possibilities during this research at Technical Institute of Gottfired Wilhelm Leibniz Universitat Hannover.

REFERENCES

1. Yun Y, Gellman AJ. Enantioselective Separation on Naturally Chiral Metal Surfaces: D,L -Aspartic Acid on Cu(3,1,17) $^{R\ \&\ S}$ Surfaces. Angew Chem Int Ed. 2013 Mar 18;52(12):3394–7. <DOI>.

2. Fujii N, Saito T. Homochirality and life. Chem Rec. 2004;4(5):267–78. <DOI>.

3. Blackmond DG. The origin of biological homochirality. Philos Trans R Soc B Biol Sci. 2011 Oct 27;366(1580):2878–84. <DOI>.

4. Sallembien Q, Bouteiller L, Crassous J, Raynal M. Possible chemical and physical scenarios towards biological homochirality. Chem Soc Rev. 2022;51(9):3436–76. <DOI>.

5. Armstrong DW, Chang CD, Li WY. Relevance of enantiomeric separations in food and beverage analyses. J Agric Food Chem. 1990 Aug;38(8):1674–7. <DOI>.

6. Nguyen LA, He H, Pham-Huy C. Chiral drugs: an overview. Int J Biomed Sci IJBS. 2006 Jun;2(2):85–100. PMID: 23674971.

7. Bachmanov AA, Bosak NP, Glendinning JI, Inoue M, Li X, Manita S, et al. Genetics of Amino Acid Taste and Appetite. Adv Nutr Int Rev J. 2016 Jul;7(4):806S-822S. <DOI>.

8. Wu Q, Lv H, Zhao L. Applications of carbon nano materials in chiral separation. Trends Anal Chem. 2020;129:115941. <DOI>.

9. Mwamwitwa KW, Kaibere RM, Fimbo AM, Sabitii W, Ntinginya NE, Mmbaga BT, et al. A retrospective cross-sectional study to

determine chirality status of registered medicines in Tanzania. Sci Rep. 2020 Dec;10(1):17834. <DOI>.

10. Kumar R. Effects of Stereoisomers on Drug Activity. Am J Biomed Sci Res. 2021 Jun 21;13(3):220–2. <DOI>.

11. Hancu G, Modroiu A. Chiral Switch: Between Therapeutical Benefit and Marketing Strategy. Pharmaceuticals. 2022 Feb 17;15(2):240. <DOI>.

12. Peepliwal A, Bagade S, Bonde C. A review: stereochemical consideration and eudismic ratio in chiral drug development. J Biomed Sci Res. 2010;2(1):29–45.

13. Genva M, Kenne Kemene T, Deleu M, Lins L, Fauconnier ML. Is It Possible to Predict the Odor of a Molecule on the Basis of its Structure? Int J Mol Sci. 2019 Jun 20;20(12):3018. <DOI>.

14. Bodák B, Breveglieri F, Mazzotti M. On the model-based design and comparison of crystallization-based deracemization techniques. Chem Eng Sci. 2022 Jun;254:117595. <DOI>.

15. Gogoi A, Mazumder N, Konwer S, Ranawat H, Chen NT, Zhuo GY. Enantiomeric Recognition and Separation by Chiral Nanoparticles. Molecules. 2019 Mar 13;24(6):1007. <DOI>.

16. Anderson NG. Developing Processes for Crystallization-Induced Asymmetric Transformation. Org Process Res Dev. 2005 Nov 1;9(6):800–13. <DOI>.

17. Robl S, Gou L, Gere A, Sordo M, Lorenz H, Mayer A, et al. Chiral separation by combining pertraction and preferential crystallization. Chem Eng Process Process Intensif. 2013 May;67:80–8. <DOI>.

18. Xie R, Chu LY, Deng JG. Membranes and membrane processes for chiral resolution. Chem Soc Rev. 2008;37(6):1243. <DOI>.

19. Liu T, Li Z, Wang J, Chen J, Guan M, Qiu H. Solid membranes for chiral separation: A review. Chem Eng J. 2021 Apr;410:128247.

20. Han H, Liu W, Xiao Y, Ma X, Wang Y. Advances of enantioselective solid membranes. New J Chem. 2021;45(15):6586–99. <DOI>.

21. Ong CS, Oor JZ, Tan SJ, Chew JW. Enantiomeric Separation of Racemic Mixtures Using Chiral-Selective and Organic-Solvent-Resistant Thin-Film Composite Membranes. ACS Appl Mater Interfaces. 2022 Mar 2;14(8):10875–85. <DOI>.

22. Tong S. Liquid-liquid chromatography in enantioseparations. J Chromatogr A. 2020 Aug;1626:461345. <DOI>.

23. Fanali S, Chankvetadze B. Some thoughts about enantioseparations in capillary electrophoresis. Electrophoresis. 2019 May 21;elps.201900144. <DOI>.

24. Bernardo-Bermejo S, Sánchez-López E, Castro-Puyana M, Marina ML. Chiral capillary electrophoresis. TrAC Trends Anal Chem. 2020 Mar;124:115807. <DOI>.

25. Ward TJ, Ward KD. Chiral Separations: A Review of Current Topics and Trends. Anal Chem. 2012 Jan 17;84(2):626–35. <DOI>.

26. Ahmed M, Kelly T, Ghanem A. Applications of enzymatic and non-enzymatic methods to access enantiomerically pure compounds using kinetic resolution and racemisation. Tetrahedron. 2012;68(34):6781–802. <DOI>.

27. Qayed WS, Aboraia AS, Abdel-Rahman HM, Youssef AF. Lipases-catalyzed enantioselective kinetic resolution of alcohols. J Chem Pharm Res. 2015;7(5):311–22.

28. Verho O, Bäckvall JE. Chemoenzymatic Dynamic Kinetic Resolution: A Powerful Tool for the Preparation of Enantiomerically Pure Alcohols and Amines. J Am Chem Soc. 2015 Apr 1;137(12):3996–4009. <DOI>.

29. Hall M. Enzymatic strategies for asymmetric synthesis. RSC Chem Biol. 2021;2(4):958–89. <DOI>.

30. Mu R, Wang Z, Wamsley MC, Duke CN, Lii PH, Epley SE, et al. Application of Enzymes in Regioselective and Stereoselective Organic Reactions. Catalysts. 2020 Jul 24;10(8):832. <DOI>.

31. Bering L, Thompson J, Micklefield J. New reaction pathways by integrating chemo- and biocatalysis. Trends Chem. 2022 May;4(5):392–408. <DOI>.

32. Burek BO, Dawood AW, Hollmann F, Liese A, Holtmann D. Process Intensification as Game Changer in Enzyme Catalysis. Front Catal. 2022;2:1–18. <DOI>.

33. Wang F, Liu Y, Du C, Gao R. Current Strategies for Real-Time Enzyme Activation. Biomolecules. 2022 Apr 19;12(5):599. <DOI>.

34. Sikora A, Siódmiak T, Marszałł MP. Kinetic Resolution of Profens by EnantioselectiveEsterification Catalyzed by *Candida antarctica* and *Candida rugosa* Lipases: Kinetic resolution of anti-inflammatory drugs. Chirality. 2014 Oct;26(10):663–9. <DOI>.

35. Kovács B, Forró E, Fülöp F. Candida antarctica lipase B catalysed kinetic resolution of 1,2,3,4-tetrahydro-ß-carbolines: Substrate specificity. Tetrahedron. 2018 Nov;74(48):6873–7. <DOI>.

36. Reetz MT. Lipases as practical biocatalysts. Curr Opin Chem Biol. 2002 Apr;6(2):145–50. <DOI>.

37. Bornscheuer UT, Bessler C, Srinivas R, Hari Krishna S. Optimizing lipases and related enzymes for efficient application. Trends Biotechnol. 2002 Oct;20(10):433–7. <DOI>.

38. Houde A, Kademi A, Leblanc D. Lipases and Their Industrial Applications: An Overview. Appl Biochem Biotechnol. 2004;118(1–3):155–70. <DOI>.

39. Bornscheuer UT, Ordoñez GR, Hidalgo A, Gollin A, Lyon J, Hitchman TS, et al. Selectivity of lipases and esterases towards phenol esters. J Mol Catal B Enzym. 2005 Nov;36(1–6):8–13. <DOI>.

40. Knežević Z, Šiler-Marinković S, Mojović L. Immobilized Lipases as Practical Catalysts. APTEFF. 2004;35:151–64. <DOI>.

41. Mojović L, Šiler-Marinković S, Kukić G, Vunjak-Novaković G. Rhizopus arrhizus lipase-catalyzed interesterification of the midfraction of palm oil to a cocoa butter equivalent fat. Enzyme Microb Technol. 1993 May;15(5):438–43. <DOI>.

42. Knezevic ZD, Siler-Marinkovic SS, Mojovic LV. Kinetics of lipase-catalyzed hydrolysis of palm oil in lecithin/izooctane reversed micelles. Appl Microbiol Biotechnol. 1998 Mar 27;49(3):267–71. <DOI>.

43. Lortie R. Enzyme catalyzed esterification. Biotechnol Adv. 1997 Jan;15(1):1–15. <DOI>.

44. Rathi P, Saxena RK, Gupta R. A novel alkaline lipase from Burkholderia cepacia for detergent formulation. Process Biochem. 2001 Oct;37(2):187–92. <DOI>.

45. Zaks A, Dodds DR. Application of biocatalysis and biotransformations to the synthesis of pharmaceuticals. Drug Discov Today. 1997 Dec;2(12):513–31. <DOI>.

46. Rasor JP, Voss E. Enzyme-catalyzed processes in pharmaceutical industry. Appl Catal Gen. 2001 Nov;221(1–2):145–58. <DOI>.

47. Zuegg J, Hönig H, Schrag JD, Cygler M. Selectivity of lipases: Conformational analysis of suggested intermediates in ester hydrolysis of chiral primary and secondary alcohols. J Mol Catal B Enzym. 1997 Jun;3(1–4):83–98. <DOI>.

48. Miyazawa T, Kurita S, Shimaoka M, Ueji S, Yamada T. Resolution of racemic carboxylic acids via the lipase-catalyzed irreversible transesterification of vinyl esters. Chirality. 1999;11(7):554–60. <DOI>.

49. Miyazawa T, Imagawa K, Yanagihara R, Yamada T. Marked dependence on temperature of enantioselectivity in the Aspergillus oryzaeprotease-catalyzed hydrolysis of amino acid esters. Biotechnol Tech. 1997;11(12):931–3. <DOI>.

50. Sandoval G, Marty A. Screening methods for synthetic activity of lipases. Enzyme Microb Technol. 2007 Feb;40(3):390–3. <DOI>.

51. Berglund P. Controlling lipase enantioselectivity for organic synthesis. Biomol Eng. 2001 Aug;18(1):13–22. <DOI>.

52. Miyazawa T, Yukawa T, Ueji S, Yanagihara R, Yamada T. Resolution of 2-phenoxy-1-propanols by Pseudomonas sp. lipase-catalyzed highly enantioselective transesterification: influence of reaction conditions on the enantioselectivity toward primary alcohols. Biotechnol Lett. 1998;20(3):235–8. <DOI>.

53. Andrade MAC, Andrade FAC, S.Phillips R. Temperature and DMSO increase the enantioselectivity of hydrolysis of methyl alkyl dimethylmalonates catalyzed by pig liver esterase. Bioorg Med Chem Lett. 1991 Jan;1(7):373–6. <DOI>.

54. Holmberg E, Hult K. Temperature as an enantioselective parameter in enzymatic resolutions of racemic mixtures. Biotechnol Lett. 1991 May;13(5):323–6. <DOI>.

55. Yasufuku Y, Ueji S ichi. Effect of temperature on lipase-catalyzed esterification in organic solvent. Biotechnol Lett [Internet]. 1995 Dec [cited 2022 Apr 2];17(12). <DOI>.

56. Phillips RS. Temperature modulation of the stereochemistry of enzymatic catalysis: Prospects for exploitation. Trends Biotechnol. 1996 Jan;14(1):13–6. <DOI>.

57. Bornscheuer U, Schapöhler S, Scheper T, Schügerl K. Influences of reaction conditions on the enantioselective transesterification using Pseudomonas cepacia lipase. Tetrahedron Asymmetry. 1991 Jan;2(10):1011–4. <DOI>.

58. Parmar VS, Prasad AK, Singh PK, Gupta S. Lipase-catalysed transesterifications using 2,2,2-trifluoroethyl butyrate: Effect of temperature on rate of reaction and enantioselectivity. Tetrahedron Asymmetry. 1992 Nov;3(11):1395–8. <DOI>.

59. Pham VT, Phillips RS. Effects of substrate structure and temperature on the stereospecificity of secondary alcohol dehydrogenase from Thermoanaerobacter ethanolicus. J Am Chem Soc. 1990 Apr;112(9):3629–32. <DOI>.

60. Eyring H. The Activated Complex in Chemical Reactions. J Chem Phys. 1935 Feb;3(2):107–15. <DOI>.

61. Straathof AJJ, Jongejan JA. The enantiomeric ratio: origin, determination and prediction. Enzyme Microb Technol. 1997 Dec;21(8):559–71. <DOI>.

62. Aydemir A. Modeling of Enzyme Catalyzed Racemic Reactions and Modifications of Enantioselectivity [Internet] [PhD Thesis]. [Hannover, Germany]: Gottfired Leibniz Universitat Hannover; 2010. Available from: <URL>.

63. Orrenius C, Hbffner F, Rotticci D, öhrner N, Norin T, Hult K. Chiral Recognition Of Alcohol Enantiomers In Acyl Transfer Reactions Catalysed By *Candida Antarctica* Lipase B. Biocatal Biotransformation. 1998 Jan;16(1):1–15. <DOI>.

64. Sih CJ, Chen CS. Microbial Asymmetric Catalysis? Enantioselective Reduction of Ketones [New Synthetic Methods (45)]. Angew Chem Int Ed Engl. 1984 Aug;23(8):570–8. <DOI>.

65. Pham VT, Phillips RS, Ljungdahl LG. Temperature-dependent enantiospecificity of secondary alcohol dehydrogenase from Thermoanaerobacter ethanolicus. J Am Chem Soc. 1989 Mar;111(5):1935–6. <DOI>.

66. Phillips RS. Temperature effects on stereochemistry of enzymatic reactions. Enzyme Microb Technol. 1992;14:417–9. <URL>.

67. Monterde MI, Brieva R, Sánchez VM, Bayod M, Gotor V. Enzymatic resolution of the chiral inductor 2-methoxy-2-phenylethanol. Tetrahedron Asymmetry. 2002 Jun;13(10):1091–6. <DOI>.

68. Lokotsch W, Fritsche K, Syldatk C. Resolution of d,l-menthol by interesterification with triacetin using the free and immobilized lipase of Candida cylindracea. Appl Microbiol Biotechnol. 1989 Oct;31–31(5–6):467–72. <DOI>.

69. Overbeeke PLA, Ottosson J, Hult K, Jongejan JA, Duine JA. The Temperature Dependence of Enzymatic Kinetic Resolutions Reveals the Relative Contribution of Enthalpy and Entropy to Enzymatic Enantioselectivity. Biocatal Biotransformation. 1998 Jan;17(1):61–79. <DOI>.

70. Ottosson J, Fransson L, Hult K. Substrate entropy in enzyme enantioselectivity: An experimental and molecular modeling study of a lipase. Protein Sci. 2002 Jun;11(6):1462–71. <DOI>.

71. Ema T. Rational strategies for highly enantioselective lipase-catalyzed kinetic resolutions of very bulky chiral compounds: substrate design and high-temperature biocatalysis. Tetrahedron Asymmetry. 2004 Sep;15(18):2765–70. <DOI>.

72. Miyazawa T, Kurita S, Ueji S, Yamada T, Kuwata S. Resolution of mandelic acids by lipase-catalysed transesterifications in organic media: inversion of enantioselectivity mediated by the acyl donor. J Chem Soc Perkin 1. 1992;(18):2253. <DOI>.

73. Ema T, Maeno S, Takaya Y, Sakai T, Utaka M. Significant effect of acyl groups on enantioselectivity in lipase-catalyzed transesterifications. Tetrahedron Asymmetry. 1996 Mar;7(3):625–8. <DOI>.

74. Lin C, Hiraga Y, Masaki K, Iefuji H, Ohkata K. Temperature-dependence of enantioselectivity and desymmetrization in the acetylation of 2-mono- and 2,2-di-substituted 1,3-propanediols by a novel lipase isolated from the yeast *Cryptococcus* spp. S-2. Biocatal Biotransformation. 2006 Jan;24(5):390–5. <DOI>.

75. Ottosson J. Enthalpy and entropy in enzyme catalysis, a study of lipase enantioselectivity [PhD Thesis]. [Department of Biotechnology, Stockholm, Sweden]: Royal Institute of Technology; 2001.

76. Yasufuku Y, Ueji S. Improvement (5-fold) of enantioselectivity for lipase-catalyzed esterification of a bulky substrate at 57 °C in organic solvent. Biotechnol Tech. 1996 Aug;10(8):625–8. <DOI>.

77. Yasufuku Y, Ueji S ichi. High Temperature-Induced High Enantioselectivity of Lipase for Esterifications of 2-Phenoxypropionic Acids in Organic Solvent. Bioorganic Chem. 1997 Apr;25(2):88–99. <DOI>.

78. Ema T, Yamaguchi K, Wakasa Y, Yabe A, Okada R, Fukumoto M, et al. Transition-state models are useful for versatile biocatalysts: kinetics and thermodynamics of enantioselective acylations of secondary alcohols catalyzed by lipase and subtilisin. J Mol Catal B Enzym. 2003 Jun;22(3–4):181–92. <DOI>.

79. Sakai T. Enhancement of the enantioselectivity in lipase-catalyzed kinetic resolutions of 3-phenyl-2H-azirine-2-methanol by lowering the temperature to -40℃. J Org Chem. 1997;62:4906–7. <URL>.

80. Sakai T, Kishimoto T, Tanaka Y, Ema T, Utaka M. Low-temperature method for enhancement of enantioselectivity in the lipase-catalyzed kinetic resolutions of solketal and some chiral alcohols. Tetrahedron Lett. 1998 Oct;39(43):7881–4. <DOI>.

81. Yang H, Jönsson Å, Wehtje E, Adlercreutz P, Mattiasson B. The enantiomeric purity of alcohols formed by enzymatic reduction of ketones can be improved by optimisation of the temperature and by using a high co-substrate concentration. Biochim Biophys Acta BBA - Gen Subj. 1997 Jul;1336(1):51–8. <DOI>.

82. Sakai T. 'Low-temperature method' for a dramatic improvement in enantioselectivity in lipase-catalyzed reactions. Tetrahedron Asymmetry. 2004 Sep;15(18):2749–56. <DOI>.

83. Majumder A, Shah S, Gupta M. Enantioselective transacetylation of (R, S)-beta-citronellol by propanol rinsed immobilized Rhizomucor miehei lipase. Chem Cent J. 2007;1:10.

84. Boutelje J, Hjalmarsson M, Hult K, Lindbäck M, Norin T. Control of the stereoselectivity of pig liver esterase by different reaction conditions in the hydrolysis of cis-N-benzyl-2,5-bismethoxycarbonylpyrrolidine and structurally related diesters. Bioorganic Chem. 1988 Dec;16(4):364–75. <DOI>.

85. Barton MJ, Hamman JP, Fichter KC, Calton GJ. Enzymatic resolution of (R,S)-2-(4-hydroxyphenoxy) propionic acid. Enzyme Microb Technol. 1990 Aug;12(8):577–83. <DOI>.

86. Cipiciani A, Bellezza F, Fringuelli F, Silvestrini MG. Influence of pH and temperature on the enantioselectivity of propan-2-ol-treated Candida rugosa lipase in the kinetic resolution of (±)-4-acetoxy-[2,2]-paracyclophane. Tetrahedron Asymmetry. 2001 Sep;12(16):2277–81. <DOI>.

87. Jurczak J, Pikul S, Bauer T. Tetrahedron report number 195 (R)- and (S)-2,3-0-isopropylideneglyceraldehyde in stereoselective organic synthesis. Tetrahedron. 1986 Jan;42(2):447–88. <DOI>.

88. Schwarz KH, Kleiner K, Ludwig R, Schrötter E, Schick H. Synthesis of methyl (±)-2,3-O-isopropylideneglycerate by electrochemical oxidation of (±)-1,2-O-isopropylideneglycerol. Liebigs Ann Chem. 1991 May 16;1991(5):503–4. <DOI>.

89. Lemaire M, Jeminet G, Gourcy JG, Dauphin G. 2- and 8-functionalized 1,4,7,10-tetraoxaspiro[5.5]undecanes. Tetrahedron Asymmetry. 1993 Jan;4(9):2101–8. <DOI>.

90. García M. Synthesis of new ether glycerophospholipids structurally related to modulator. Tetrahedron. 1991;47(48):10023–34. <DOI>.

91. Dröge MJ, Bos R, Woerdenbag HJ, Quax WJ. Chiral gas chromatography for the determination of 1,2-O-isopropylidene-sn-glycerol stereoisomers. J Sep Sci. 2003 Jul 1;26(9–10):771–6. <DOI>.

92. Lundh M, Nordin O, Hedenström E, Högberg HE. Enzyme catalysed irreversible transesterifications with vinyl acetate. Are they really irreversible? Tetrahedron Asymmetry. 1995 Sep;6(9):2237–44. <DOI>.

93. Secundo F, Ottolina G, Riva S, Carrea G. The enantioselectivity of lipase PS in chlorinated solvents increases as a function of substrate conversion. Tetrahedron Asymmetry. 1997 Jul;8(13):2167–73. <DOI>.

94. Zanoni G, Agnelli F, Meriggi A, Vidari G. Enantioselective syntheses of isoprostane and iridoid lactones intermediates by enzymatic transesterification. Tetrahedron Asymmetry. 2001 Jul;12(12):1779–84. <DOI>.

95. Bornscheuer U, Stamatis H, Xenakis A, Yamane T, Kolisis FN. A comparison of different strategies for lipase-catalyzed synthesis of partial glycerides. Biotechnol Lett. 1994 Jul;16(7):697–702. <DOI>.

96. Tservistas M. Untersuchungen zum Einsatz von überkritischem Kohlendioxid als Medium für biokatalysierte Reaktionen [Dissertation]. [Hannover, Germany]: Leibniz Universität Hannover; 1997.

97. Capewell A, Wendel V, Bornscheuer U, Meyer HH, Scheper T. Lipase-catalyzed kinetic resolution of 3-hydroxy esters in organic solvents and supercritical carbon dioxide. Enzyme Microb Technol. 1996 Aug;19(3):181–6. <DOI>.

98. Yildirim A. Lipase Catalysed Transesterification of Isopropyledene Glycerol [Master of Science Thesis]. [Hannover, Germany]: Gottfired Leibniz Universitat Hannover; 2005.

99. Chen CS, Sih CJ. General Aspects and Optimization of Enantioselective Biocatalysis in Organic Solvents: The Use of Lipases[New Synthetic Methods(76)]. Angew Chem Int Ed Engl. 1989 Jun;28(6):695–707. <DOI>.

100. Rakels JLL, Straathof AJJ, Heijnen JJ. A simple method to determine the enantiomeric ratio in enantioselective biocatalysis. Enzyme Microb Technol. 1993 Dec;15(12):1051–6. <DOI>.

101. Persson M, Costes D, Wehtje E, Adlercreutz P. Effects of solvent, water activity and temperature on lipase and hydroxynitrile lyase enantioselectivity. Enzyme Microb Technol. 2002 Jun;30(7):916–23. <DOI>.